

Conditional Flow Matching: Simulation-Free Dynamic Optimal Transport

Alexander Tong¹ Nikolay Malkin¹ Guillaume Huguet¹ Yanlei Zhang¹ Jarriid Rector-Brooks¹ Kilian Fatras²
Guy Wolf¹ Yoshua Bengio^{1,3}

Abstract

Continuous normalizing flows (CNFs) are an attractive generative modeling technique, but they have thus far been held back by limitations in their simulation-based maximum likelihood training. In this paper, we introduce a new technique called *conditional flow matching* (CFM), a simulation-free training objective for CNFs. CFM features a stable regression objective like that used to train the stochastic flow in diffusion models but enjoys the efficient inference of deterministic flow models. In contrast to both diffusion models and prior CNF training algorithms, our CFM objective does not require the source distribution to be Gaussian or require evaluation of its density. Based on this new objective, we also introduce *optimal transport CFM* (OT-CFM), which creates simpler flows that are more stable to train and lead to faster inference, as evaluated in our experiments. Training CNFs with CFM improves results on a variety of conditional and unconditional generation tasks such as inferring single cell dynamics, unsupervised image translation, and Schrödinger bridge inference. Code is available at <https://github.com/atong01/conditional-flow-matching>.

1. Introduction

Generative modeling considers the problem of approximating and sampling from a probability distribution. Normalizing flow techniques, which have emerged as a competitive generating modeling method, construct an invertible and efficiently differentiable mapping between a fixed (e.g., standard normal) distribution and the target distribution (Rezende & Mohamed, 2015). They are powerful density estimators and allow efficient transformation of the standard normal distribution to the data distribution.

While original normalizing flow work expressed transfor-

¹Mila – Québec AI Institute and Université de Montréal ²Mila – Québec AI Institute and McGill University ³CIFAR Fellow. Correspondence to: Alexander Tong <alexander.tong@mila.quebec>.

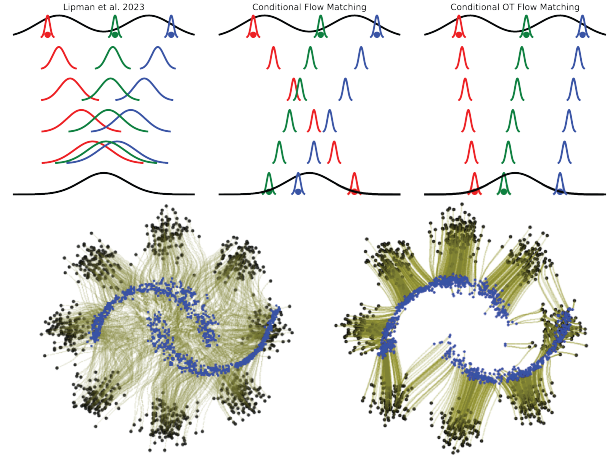


Figure 1. **Above:** Conditional flows from (a) Lipman et al. (2022) which is restricted to generating from the normal distribution, (b) the proposed Conditional Flow Matching (CFM) and (c) its variant Optimal Transport Conditional Flow Matching (OT-CFM). **Below:** Learned flows (green) from moons (blue) to 8-Gaussians (black) using CFM (left) and OT-CFM (right), not possible using FM.

mations as static compositions of invertible modules, a continuous-time variant of normalizing flows, termed continuous normalizing flows (CNFs), was developed in Chen et al. (2018). The notable difference is that CNFs’ invertible mapping between distributions is specified by a neural ordinary differential equation (ODE). Unfortunately, CNFs exhibit training difficulties and do not scale well to large-scale datasets (Chen et al., 2018; Grathwohl et al., 2019; Onken et al., 2021).

Meanwhile, diffusion models, which are the current state of the art on many generative modeling tasks (Dhariwal & Nichol, 2021; Austin et al., 2021; Corso et al., 2022; Watson et al., 2022b), generate new samples by simulating a stochastic differential equation (SDE) that transforms a simple density to the data distribution. Diffusion models owe their success in part to their simple regression training objective, which does not require simulating the SDE during training. Recently, Lipman et al. (2022) showed that CNFs could also be trained using *flow matching* (FM), a direct regression of the flow (ODE drift) similar to training of diffusion models. FM was shown to produce high-quality samples and stabilize CNF training.

One of the major drawbacks of both CNF (ODE) and diffusion (SDE) models compared to other generative models (e.g., variational autoencoders (Kingma & Welling, 2014), (discrete-time) normalizing flows, and generative adversarial networks (Goodfellow et al., 2014)), is a comparatively long inference time. Flow models can require many passes through the network to generate a high-quality sample. Defining CNFs which enjoy both the fast inference of normalizing flows and stable training of diffusion models is an open problem and one of the motivations for this work.

In this work we introduce a general class of objectives for CNFs which we call *conditional flow matching* (CFM). Like FM, CFM allows for training of continuous-time flow models without integration or backpropagation through time. Further, because the flow is parametrized by an ODE, we can use efficient ODE solvers at inference time, avoiding solving a SDE as required in diffusion models. CFM is also more flexible than FM as it can be trained using arbitrary source distributions and meaningful regularizations, whereas FM must use a Gaussian source distribution and admits no simple regularization mechanisms.

Inspired by prior work on enforcing an optimal transport (OT) property in flow models (Tong et al., 2020; Finlay et al., 2020; Onken et al., 2021), we also propose *optimal transport conditional flow matching* (OT-CFM), a variant of CFM which approximates a dynamic OT map between the source and target distribution in a simulation-free manner. We show that this leads to more accurate OT flows than existing neural OT models based on ODEs (Tong et al., 2020; Finlay et al., 2020), SDEs (De Bortoli et al., 2021; Vargas et al., 2021), or input convex neural networks (ICNNs) (Makkuva et al., 2020). Furthermore, we show variants of OT-CFM can be used to train an ODE to match the probability flow of a Schrödinger bridge with a Brownian motion reference process.

In summary, our main contributions are as follows:

- (1) We introduce a novel class of objectives called *conditional flow matching*. CFM is able to learn conditional generative models from any sampleable source distribution, generalizing models previously restricted to a Gaussian source by conditioning on paired source and target samples.
- (2) We strengthen CFM by drawing source and target samples according to an optimal transport plan, allowing us to reformulate the learning problem into a constrained optimization of Dynamic OT or a Schrödinger bridge between distributions.
- (3) We evaluate our proposed CFM and OT-CFM in experiments on single cell dynamics, unsupervised image translation, energy-based models, and Schrödinger bridge problems. Our experiments show that the OT-CFM objective leads to more efficient training and decreases inference time.

The paper is organized as follows. In §2 and §3 we define the background and mathematical ingredients needed to introduce our new methods. In §4, we define CFM and OT-CFM. We discuss the related work in §5. Finally in §6, we extensively evaluate our new methods.

2. Mathematical Background

In this section, we define all the background needed to present our new methods.

Notations. We consider the setting of data defined in \mathbb{R}^d with (possibly unknown) densities $q(x_0)$ and $q(x_1)$ (also denoted q_0, q_1) at times $t = 0$ and $t = 1$ respectively defined over $\mathcal{X} \subseteq \mathbb{R}^d$. We may have access to samples from these distributions denoted $\mathbf{X}_{\{0,1\}}$ or access to the unnormalized energy functions $E(x) : \mathbb{R}^d \rightarrow \mathbb{R}^+$ where $q(x) = E(x)/Z$ for some normalizing constant $Z = \int_{\mathcal{X}} E(x)dx$.

Continuous probability flows. We consider a time dependent probability path $p : [0, 1] \times \mathbb{R}^d \rightarrow \mathbb{R}^+$ and a time dependent vector field $v : [0, 1] \times \mathbb{R}^d \rightarrow \mathbb{R}^d$. To ensure the uniqueness of integral curves (thus corresponding flow), we assume the regularity of vector field v is at least (locally) Lipschitz on x and Bochner integrable on t . This vector field defines a unique time dependent flow $\phi : [0, 1] \times \mathbb{R}^d \rightarrow \mathbb{R}^d$ defined via an ordinary differential equation (ODE):

$$\frac{d\phi_t(x)}{dt} = v_t(\phi_t(x)); \quad \phi_0(x) = x \quad (1)$$

which subsequently defines a push-forward $\phi_{\#} : [0, 1] \times \mathcal{P}(\mathbb{R}^d) \rightarrow \mathcal{P}(\mathbb{R}^d)$ which pushes a density forward over time

$$p_t(x) = [\phi_t]_{\#} p_0(x) = p_0(\phi^{-1}(x)) |\det \nabla_x \phi_t^{-1}(x)| \quad (2)$$

which satisfies the property that for any measurable set $B \subset \mathbb{R}^d$, $p_t(B) = p_0(\phi^{-1}(B))$. If some ϕ_t solves eq. 1 for all $x \in X$, we say that v_t generates ϕ_t . When $p_0(x) = \mathcal{N}(x | 0, 1)$ and $[\phi_1]_{\#}$ is parameterized by a neural network then we recover the normalizing flow (NF) (Rezende & Mohamed, 2015) framework and when ϕ_t is parametrized by a neural network we recover the continuous normalizing flow (CNF) framework (Chen et al., 2018).

Optimal transport. The optimal transport problem seeks the minimal displacement cost from one measure to another by relying on a given ground cost. Formally, we define the 2-Wasserstein distance, with respect to a non-negative ground cost $c(\cdot, \cdot)$, by

$$W(q_0, q_1)_2^2 = \inf_{\pi \in \Pi} \int_{\mathcal{X}^2} c(x, y)^2 \pi(dx, dy), \quad (3)$$

where Π denotes the set of all joint probability measures on \mathcal{X}^2 whose marginals are q_0 and q_1 . The dynamic form of

the 2-Wasserstein distance is given by

$$W(q_0, q_1)_2^2 = \inf_{p_t, u_t} \int_{\mathbb{R}^d} \int_0^1 p_t(x) \|u_t(x)\|^2 dt dx, \quad (4)$$

with $p_t \geq 0$ and subject to the boundary conditions $p_0 = q_0$, $p_1 = q_1$ and the continuity equation $\partial_t p_t + \nabla \cdot (p_t u_t) = 0$. Tong et al. (2020); Finlay et al. (2020) showed that CNFs with squared L^2 regularization approximate dynamic optimal transport. For general marginals, however, these models required integrating over and backpropagating through tens to hundreds of function evaluations, resulting in both numerical and efficiency issues. We aim to avoid these issues by directly regressing the flow like Flow Matching methods.

Optimal transport is also related to the Schrödinger bridge (SB) problem (Léonard, 2014b). We show in §4.4 that a variant of the algorithm we propose recovers the probability flow of the solution to a SB problem with a Brownian noise reference process.

Gaussian marginal conditional flows. When marginals are Gaussian conditioned on some random variable z , then the flow ϕ_t and the vector field that generates that flow u_t can be solved in closed form. Consider the time-dependent Gaussian conditional path where $p_t(x|z) = \mathcal{N}(x|\mu_t(z), \sigma_t^2(z))$. While there are many flows that generate this probability path, one of the simplest is

$$\phi_{t,z}(x) = \mu_t(z) + \sigma_t(z)x, \quad (5)$$

which is also consistent with the dynamic optimal transport (OT) flow (Peyré & Cuturi, 2019). As previously shown there is a unique vector field that generates $\phi_{t,z}$.

Theorem 2.1 (Theorem 3 Lipman et al. (2022)). *The unique vector field that generates $\phi_{t,z}$ in eq. 5 has the form*

$$u_t(x|z) = \frac{\sigma'_t(z)}{\sigma_t(z)}(x - \mu_t(z)) + \mu'_t(z). \quad (6)$$

where $\sigma'_t(z)$ and $\mu'_t(z)$ denote the time derivative of $\sigma_t(z)$ and $u_t(z)$ respectively and $u_t(x|z)$ generates the Gaussian marginal path $p_t(x|z)$.

Lipman et al. (2022) used this closed form for fast generation by conditioning on a datapoint x_1 and considering the path back to $\mathcal{N}(0, 1)$ for each datapoint (see Figure 1).

3. The Conditional Flow Matching Framework

Assume we are given a target flow p_t and a vector field u_t that generates it. One way to learn a flow that matches p_t is through gradient descent on regression against the target vector field. We call this *Flow Matching* following Lipman et al. (2022). Specifically, we would like to learn a time dependent parameterized vector field $v_\theta(t, x) : [0, 1] \times$

Algorithm 1 Conditional Flow Matching

Input: Efficiently sampleable $q(z)$, $p_t(x|z)$, and computable $u_t(x|z)$ and initial network v_θ .

while Training **do**

$z \sim q(z); \quad t \sim \mathcal{U}(0, 1)$
 $x \sim p_t(x|z)$
 $L_{CFM}(\theta) \leftarrow \|v_\theta(t, x) - u_t(x|z)\|^2$
 $\theta \leftarrow \text{Update}(\theta, \nabla_\theta L_{CFM}(\theta))$

return v_θ

$\mathbb{R}^d \rightarrow \mathbb{R}^d$ by regression against some target vector field $u_t(x) : [0, 1] \times \mathbb{R}^d \rightarrow \mathbb{R}^d$ by minimizing a flow matching (FM) loss

$$L_{FM}(\theta) = \mathbb{E}_{t, p_t(x)} \|v_\theta(t, x) - u_t(x)\|_2^2 \quad (7)$$

For most interesting problems $u_t(x)$ is computationally intractable to compute directly. To get around this, we consider u_t that can be learned from a mixture of simpler flows.

3.1. Constructing p_t, u_t from Conditionals

A simple way of constructing a probability path is via a mixture of conditional probability paths. Specifically, for any condition z independent of x and t it is clear that

$$p_t(x) = \int p_t(x|z)q(z)dz. \quad (8)$$

We consider the case where the boundary conditions at $t = 0$ (resp. $t = 1$), p_0 (resp. p_1) closely approximate the distribution q_0 (resp. q_1). Similarly, we can also define our marginal vector field, by marginalizing over conditional vector fields conditioned on z i.e.

$$u_t(x) = \mathbb{E}_{q(z)} \frac{u_t(x|z)p_t(x|z)}{p_t(x)} \quad (9)$$

where $u_t(x|z) : \mathbb{R}^d \rightarrow \mathbb{R}^d$ is a conditional vector field that generates $p_t(x|z)$ from $p_0(x|z)$. Interestingly, when defined this way, we can also show that u_t generates p_t under some mild conditions.

Theorem 3.1. *The marginal vector field (eq. 9) generates the marginal probability path (eq. 8) from $p_0(x)$ given any $q(z)$ independent of x and t .*

All proofs appear in Appendix A. This surprising result extends Lipman et al. (2022, Theorem 1) to more general conditionings and delineates some minor conditions on $q(z)$. It follows from showing p_t, u_t satisfy the continuity equation for $t \in [0, 1]$.

3.2. Conditional Flow Matching

Surprisingly, we can get an unbiased estimator of the marginal through the conditional flow matching (CFM) objective:

$$L_{CFM}(\theta) = \mathbb{E}_{t, q(z), p_t(x|z)} \|v_\theta(t, x) - u_t(x|z)\|_2^2. \quad (10)$$

Table 1. Summary of probability path definitions for existing conditional flow matching (top) and our newly defined paths (bottom). We define three new probability path objectives that can handle general source distributions and optimal transport flows.

Probability Path	$q(z)$	$\mu_t(z)$	σ_t	Cond. OT	Marginal OT	General source
Var. Exploding (Song & Ermon, 2019)	$q(x_1)$	x_1	σ_{1-t}	No	No	No
Var. Preserving (Ho et al., 2020)	$q(x_1)$	$\alpha_{1-t}x_1$	$\sqrt{1 - \alpha_{1-t}^2}$	No	No	No
Flow Matching (Lipman et al., 2022)	$q(x_1)$	tx_1	$t\sigma - t + 1$	Yes	No	No
Source Conditional Flow Matching (CFM)	$q(x_0)q(x_1)$	$tx_1 + (1-t)x_0$	$\sqrt{(\sigma t)^2 + 2\sigma t(1-t)}$	No	No	Yes
Conditional Flow Matching	$q(x_0)q(x_1)$	$tx_1 + (1-t)x_0$	σ	Yes	No	Yes
Optimal Transport CFM	$\pi(x_0, x_1)$	$tx_1 + (1-t)x_0$	σ	Yes	Yes	Yes
Schrödinger Bridge CFM	$\pi_{2\sigma^2}(x_0, x_1)$	$tx_1 + (1-t)x_0$	$\sigma\sqrt{t(1-t)}$	Yes	Yes	Yes

The CFM objective describes how to regress against the marginal flow with access only to samples from the conditional probability path and conditional vector fields. This is formalized in the following theorem.

Theorem 3.2. *Assuming that $p_t(x) > 0$ for all $x \in \mathbb{R}^d$ and $t \in [0, 1]$ and $q(z)$ independent of x and t , then, up to a constant independent of θ , L_{CFM} and L_{FM} are equal. Hence,*

$$\nabla_{\theta} L_{FM}(\theta) = \nabla_{\theta} L_{CFM}(\theta) \quad (11)$$

This is useful when the marginal vector field u_t is intractable but the conditional vector field $u_t(x|z)$ is simple. Using this transformation, as long as we can efficiently sample from $q(z)$, $p_t(x|z)$ and calculate $u_t(x|z)$, we can then perform flow matching of the marginals.

4. Conditional Flow Matching Variants

In this section, we introduce multiple forms of conditional flow matching depending on the choices of $q(z)$, $p_t(\cdot|z)$, and $u_t(\cdot|z)$ which are summarized in Table 1 (bottom). We first show how that the formulation of Lipman et al. (2022) from $q(x_0) = \mathcal{N}(x | 0, 1)$ fits into this framework. In order to alleviate the Gaussian source requirement, we next condition on a pair of points $(x_0, x_1) \sim (q_0, q_1)$ which we call conditional flow matching. To generalize the CFM objective, we introduce an OT map between the source and target distributions as an additional condition, which enforces the marginal flow to be an OT flow. Next we introduce a flow conditioned on an entropy regularized OT map that solves the Schrödinger bridge problem. Finally, we introduce two ways to lower variance of the target which can improve training speed.

4.1. FM from the Gaussian

Lipman et al. (2022) consider the problem of unconditional generative modeling from a training dataset. Here z is a single datapoint $z := x_1$ sampled uniformly from the data that is $q(z) := p_{\text{data}}$, and for some small constant $\sigma \in \mathbb{R}^+$,

$$p_t(x|z) = \mathcal{N}(x | tx_1, (t\sigma - t + 1)^2), \quad (12)$$

$$u_t(x|z) = \frac{x_1 - (1 - \sigma)x}{1 - (1 - \sigma)t}. \quad (13)$$

As shown in Lipman et al. (2022) the conditional flow is an optimal transport flow from the standard normal distribution to a Gaussian distribution centered at x_1 with standard deviation σ . However, the unconditional flow u_t is *not* an optimal transport flow between the standard normal and the training data.

Interestingly, there exists a set of conditional probability paths conditioned on x_1 and $x_0 \sim \mathcal{N}(0, 1)$ that have an equivalent probability flow to the marginal p_t of flow matching which is only conditioned on x_1 which we call *source conditional flow matching* which uses the conditional probability path

$$p_t(x|z) = \mathcal{N}(x | tx_1 + (1-t)x_0, (\sigma t)^2 + 2\sigma t(1-t)).$$

This relationship to flow matching is formalized in Prop. A.1. Conditioning on x_0 will allow us to move away from normalizing flow models to more general flow.

4.2. Simplified CFMs

The previous source conditional flow matching objective has a somewhat strange σ_t which is an artifact of using a Gaussian around the target point x_1 and is neither a conditional nor marginal optimal transport flow. Formally, let z be a tuple of random variables $z := (x_0, x_1)$ where x_0 and x_1 are sampled from q_0 and q_1 , and let the conditionals be Gaussian flows between x_0 and x_1 with standard deviation σ , we thus have

$$q(z) = q(x_0)q(x_1), \quad (14)$$

$$p_t(x|z) = \mathcal{N}(x | tx_1 + (1-t)x_0, \sigma^2), \quad (15)$$

$$u_t(x|z) = x_1 - x_0. \quad (16)$$

We note that the formulation of $u_t(x|z)$ follows from an application of Theorem 2.1 to the probability path $\mu_t = tx_1 + (1-t)x_0$ and $\sigma_t = \sigma$. Further, we note that $p_t(x|z)$ is efficiently sampleable and u_t is efficiently computable, thus gradient descent on L_{CFM} is also efficient. For this choice of z , $p_t(\cdot|z)$, and $u_t(\cdot|z)$, we know the marginal boundary probabilities approach q_0 and q_1 respectively as $\sigma \rightarrow 0$. This is made explicit in the following Proposition, where $*$ denotes the convolution operator.

Proposition 4.1. *The marginal p_t corresponding to $q(z)$, $p_t(x|z)$, and $u_t(x|z)$ in eqs. 14-16 has boundary conditions $p_1 = q_1 * \mathcal{N}(x | 0, \sigma^2)$ and $p_0 = q_0 * \mathcal{N}(x | 0, \sigma^2)$.*

This shows that CFM strictly generalizes FM in the sense that it has equivalent probability paths for a Gaussian source, but can be generalized to any sample-able q_0 . Additionally, while each conditional flow is still the dynamical optimal transport flow from x_0 to x_1 , the marginal flow is still not an optimal transport flow.

4.3. Optimal Transport CFM

However, we can achieve dynamic optimal transport with the addition of a static optimal transport step. Let π be a 2-Wasserstein optimal transport map with marginals q_0, q_1 as in eq. 3. In this case z is still a tuple of points, but instead of being sampled uniformly from the joint distribution $q_0 q_1$, z is sampled according to π , that is

$$q(z) := \pi(x_0, x_1) \quad (17)$$

we use the same $p_t(x|z)$ in eq. 15 and $u_t(x|z)$ in eq. 16. In this case, OT-CFM is equivalent to dynamic optimal transport in the following sense.

Proposition 4.2. *The results of Prop. 4.1 also hold for $q(z)$ in eq. 17. Furthermore, as $\sigma^2 \rightarrow 0$ the marginal path p_t and field u_t are the unique minimizers of eq. 4, i.e., u_t solves the dynamic optimal transport problem between q_0 and q_1 .*

For large datasets, π can be difficult to compute and store (Cuturi, 2013; Tong et al., 2020). For this reason we use a minibatch computation of OT similar to Fatras et al. (2021b). Specifically, we perform OT for each batch of data during training and sample points from π_{batch} equal to the number of points in the batch.¹ As the OT batch size equals the support of (q_0, q_1) , we recover Prop. 4.2 and the exact dynamic optimal transport. We show empirically that the batch size can be much smaller in many cases, which aligns with prior studies (Fatras et al., 2020; 2021a).

4.4. Schrödinger Bridge Probability Flow

Recently, there has been significant effort in learning diffusion models with more general source distributions formulated as a Schrödinger bridge problem (De Bortoli et al., 2021; Vargas et al., 2021). Here we show that a SB-CFM, a variant of OT-CFM, can be used to train an ODE to match the probability flow of a Schrödinger bridge with a Brownian motion reference process.

Let p_{ref} be the standard Wiener process scaled by σ with initial-time marginal $p_{ref}(x_0) = q(x_0)$. The Schrödinger bridge problem (Schrödinger, 1932) seeks the process π that is closest to p_{ref} while having initial and terminal marginal

¹In general the OT batch size need not match the optimization batch size, but we keep them equal for simplicity.

distributions specified by the data distribution $q(x_0)$ and $q(x_1)$:

$$\pi^* := \arg \min_{\pi(x_0)=q(x_0), \pi(x_1)=q(x_1)} \text{KL}(\pi \| p_{ref}). \quad (18)$$

We define the joint distribution

$$q(z) := \pi_{2\sigma^2}(x_0, x_1) \quad (19)$$

where $\pi_{2\sigma^2}$ is the solution of the entropy-regularized optimal transport problem (Cuturi, 2013) with cost $\|x_0 - x_1\|$ and entropy regularization $\lambda = 2\sigma^2$ in eq. 31. We set the conditional path distribution to be a Brownian bridge with diffusion scale σ between x_0 and x_1 , with probability flow and generating vector field

$$p_t(x|z) = \mathcal{N}(x | tx_1 + (1-t)x_0, t(1-t)\sigma^2) \quad (20)$$

$$u_t(x|z) = \frac{1-2t}{2t(1-t)}(x - (tx_1 + (1-t)x_0)) + (x_1 - x_0), \quad (21)$$

where u_t is given by eq. 6. The marginal coupling $\pi_{2\sigma^2}$ and $u_t(x|z)$ define $u_t(x)$, which is approximated by the regression objective in Algorithm 4.

Proposition 4.3. *The flow $u_t(x)$ defined by eq. 19 and eq. 21 generates the same marginal probability path as the solution π^* to the Schrödinger bridge problem in eq. 18.*

4.5. Lower Variance Flow Estimates

An interesting consequence of introducing optimal transport to conditional flow matching is that it greatly reduces variance of the regression target. Informally, as $\sigma \rightarrow 0$, $\mathbb{E}_{x,t,z} \|u_t(x|z) - u_t(x)\|^2 \rightarrow 0$ for OT-CFM and SB-CFM, which is not true of previous probability paths in Table 1 (See Proposition A.2 for a precise statement). As flow models get larger, more powerful, and more costly, reducing objective variance, and thereby faster training may lead to significant cost savings (Watson et al., 2022b). To this end we also explore reducing the variance of the objective by averaging over a batch. This is not feasible in score matching where the flow conditioned on multiple datapoints is complex. Our CFM framework naturally extends from a pair of datapoints to a batch of pairs. Instead of conditioning on a single pair of datapoints we can condition on a batch of pairs. As the batch increases in size, we trade higher cost in computing the target for lower variance in the target as the batch size increases, the variance in the target goes to zero (see Proposition A.3 for a precise statement).

5. Related Work

Prior work considering simulation-free training of CNFs involve difficult to estimate integrals, biased gradients, and only the standard normal source distribution (Rozen et al., 2021; Ben-Hamu et al., 2022; Lipman et al., 2022). In contrast, simulation-free training is common in stochastic flow

models where backpropagating through the simulation is numerically challenging and has high variance (Li et al., 2020). While these diffusion models have recently achieved exceptional generative performance on many tasks (Sohl-Dickstein et al., 2015; Song & Ermon, 2019; 2020; Ho et al., 2020; Song et al., 2021b; Dhariwal & Nichol, 2021; Watson et al., 2022b), their simulation requires an inherently costly SDE simulation with many follow-up works to improve inference efficiency (Lu et al., 2022; Salimans & Ho, 2022; Watson et al., 2022a; Song et al., 2021a; Bao et al., 2022). These methods generally consider a simple Gaussian diffusion process, and do not consider generalizing the source distribution. Other works consider general source distribution but this makes the optimization and inference more challenging, needing multiple iterations or other tricks to perform well (Wang et al., 2021; De Bortoli et al., 2021; Vargas et al., 2021).

There are a variety of methods that consider optimal transport between continuous distributions with neural networks; however, these require constrained architectures (Leygonie et al., 2019; Makkuva et al., 2020; Bunne et al., 2022), or use a regularized CNF which is challenging to optimize (Tong et al., 2020; Finlay et al., 2020; Onken et al., 2021; Huguette et al., 2022a). With our work it is possible to achieve optimal transport flows without either of these constraints as we show empirically in the next section.

6. Results

In this section we empirically evaluate the CFM and OT-CFM objectives with respect to both optimal transport and generative modeling criteria. We show that OT-CFM leads to more efficient training and inference. We also compare SB-CFM to baselines and discuss extensions of the proposed algorithms to learning from unnormalized target densities. All experiment details can be found in §D.

6.1. Optimal Transport and Faster Convergence

We start by evaluating how well various neural OT models perform optimal transport in low dimensions.² Table 2 summarizes our results showing that OT-CFM flows generalize better to the test set and are very close to the dynamic optimal transport paths as measured by normalized path energy. We find transforming moons \leftrightarrow 8gaussians to be particularly challenging to learn for CFM as compared to OT-CFM, the learned paths are depicted in Figure 1 (bottom).

OT-CFM matches a minibatch-OT map, which is equivalent to the optimal transport when batch size $\rightarrow \infty$ and to a

²To measure how well a model solves the OT problem we use normalized path energy (NPE), defined via the 2-Wasserstein distance as $\text{NPE}(v_\theta) = |PE(v_\theta) - W_2^2(q_0, q_1)| / W_2^2(q_0, q_1)$, where the path energy (PE) is $PE(v_\theta) = \mathbb{E}_{x(0) \sim q(x_0)} \int_0^1 \|v_\theta(t, x(t))\|^2 dt$.

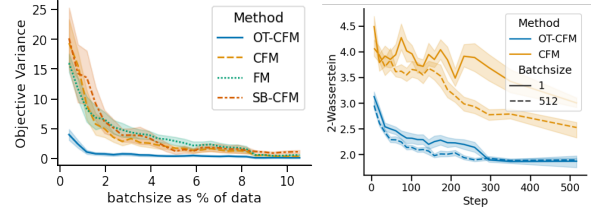


Figure 2. (left) Variance of the objective for varying batch size. OT-CFM has a lower variance across batch sizes. (right) Validation 2-Wasserstein performance with batch averaging as in §4.5. Reducing variance improves training efficiency.

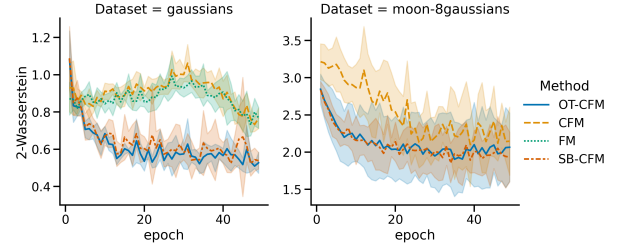


Figure 3. OT-CFM trains faster in terms of validation set error than CFM and FM models.

random alignment as batch size $\rightarrow 1$. We find that OT-CFM requires surprisingly small batches to approximate the OT map well, suggesting some generalization advantages of the network optimization (Figure S2).

Reducing variance in the target. We next consider the variance of the objective $u_t(x|z)$ with respect to z . While for any x we have $\mathbb{E}_q(z)u_t(x|z) = u_t(x)$, we find a lower second moment speeds up training. Specifically, we seek to understand the effect of the second moment which we call the *objective variance* defined as

$$OV = \mathbb{E}_{t \sim U(0,1), x \sim p_t(x), z \sim q(z)} \|u_t(x|z) - u_t(x)\|^2 \quad (22)$$

on training speed for different objectives in Table 1. We estimate the variance on a small data with a known $u_t(x)$. We examine this estimated objective variance and its effect on training convergence in Figure 2, showing that either OT-CFM or variance reduced CFM with averaging over the batch results in lower variance of the objective. This in turn leads to faster training times as shown on the right. Averaging over a batch of data leads to faster training particularly for methods with high objective variance (CFM) and less so for those with low (OT-CFM), which already trains quickly.

Faster training. By conditioning on minibatch optimal transport flows, OT-CFM is substantially easier to train which we posit is due to the variance reduction of the conditional flow. In Figure 3 we evaluate the performance over time of OT-CFM against CFM and FM objectives. For the same number of steps OT-CFM has better performance on the validation set. In Table S1 we compare the training times for various Neural OT methods whose performance can be

Table 2. Comparison of neural optimal transport methods over four datasets and with $(\mu \pm \sigma)$ over five seeds in terms of fit (2-Wasserstein), optimal transport performance (normalized path energy), and Runtime. ‘—’ indicates a method that requires a Gaussian source. Best in **bold**. CFM and DSB are trained on a single CPU core, other baselines are trained with a GPU and two CPUs.

	Test 2-Wasserstein Error (\downarrow)				Normalized Path Energy (\downarrow)				Train time (s) $\times 10^3$
	8gaussians	moons-8gaussians	moons	scurve	8gaussians	moons-8gaussians	moons	scurve	Avg.
OT-CFM	1.262 \pm 0.348	1.923 \pm 0.391	0.239 \pm 0.048	0.264 \pm 0.093	0.018 \pm 0.014	0.053 \pm 0.035	0.087 \pm 0.061	0.027 \pm 0.026	1.484 \pm 0.192
CFM	1.284 \pm 0.384	1.977 \pm 0.266	0.338 \pm 0.109	0.333 \pm 0.060	0.222 \pm 0.032	2.738 \pm 0.181	0.841 \pm 0.148	0.867 \pm 0.117	1.046 \pm 0.132
FM	1.062 \pm 0.196	—	0.246 \pm 0.077	0.377 \pm 0.099	0.174 \pm 0.030	—	0.778 \pm 0.144	0.772 \pm 0.081	1.014 \pm 0.170
Reg. CNF	1.144 \pm 0.075	—	0.376 \pm 0.040	0.581 \pm 0.195	0.274 \pm 0.060	—	0.620 \pm 0.088	0.586 \pm 0.503	8.021 \pm 3.288
CNF	1.055 \pm 0.059	—	0.387 \pm 0.065	0.645 \pm 0.343	0.151 \pm 0.064	—	2.937 \pm 1.973	10.548 \pm 8.100	18.810 \pm 12.677
ICNN	1.771 \pm 0.398	2.193 \pm 0.136	0.532 \pm 0.046	0.753 \pm 0.068	0.747 \pm 0.029	0.832 \pm 0.004	0.267 \pm 0.010	0.344 \pm 0.045	2.912 \pm 0.626

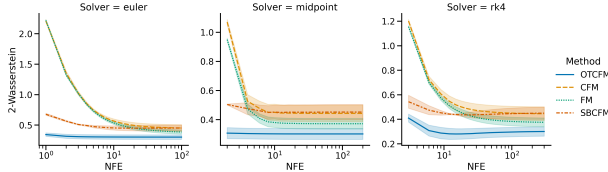


Figure 4. With different ODE integrators, OT-CFM reduces the error for a fixed number of function evaluations during inference.

seen in Table 2. Simulation-free optimization is significantly faster to train with equal or superior performance.

Faster inference. We next evaluate the quality of samples during inference time. In Figure 4, we compare the quality of samples for different number of function evaluations (NFEs) across different flow matching objectives. In this experiment we sample from the source distribution test set and simulate the ODE over time for different solvers. We find that OT-CFM consistently requires fewer evaluations to achieve the same quality and achieves better quality with the same NFEs. This is consistent with previous work which found OT paths lead to faster, higher quality inference in regularized CNFs (Finlay et al., 2020; Onken et al., 2021) and flow matching vs. standard variance preserving and variance exploding probability paths (Lipman et al., 2022).

Single-cell interpolation. Next we consider the task of single-cell trajectory interpolation. In this task we use leave-one-out validation over the timepoints. From times data at times $[0, t - 1], [t + 1, T]$ we try to interpolate its distribution at time t following the setup of Schiebinger et al. (2019); Tong et al. (2020); Huguet et al. (2022a). Low error means we model individual cells well, which is useful in a number of downstream tasks such as gene regulatory network inference (Aliee et al., 2021; Yeo et al., 2021). Following Huguet et al. (2022b), we repurpose the CITE-seq and Multiome datasets from a recent NeurIPS competition for this task (Burkhardt et al., 2022). We also include the Embryoid-body data from Moon et al. (2019); Tong et al. (2020). Table 3 shows the average earth mover’s distance (1-Wasserstein) on left out timepoints for three datasets. On all three datasets OT-CFM outperforms other methods and baselines on average.

Table 3. Single-cell comparison over three datasets averaged over leaving out intermediate timepoints measuring EMD to left out distribution following Tong et al. (2020). *Indicates values taken from aforementioned work.

Dataset	Cite	EB	Multi
OT-CFM	0.882 \pm 0.058	0.790 \pm 0.068	0.937 \pm 0.054
CFM	0.965 \pm 0.111	0.872 \pm 0.087	1.085 \pm 0.099
SB-CFM	1.067 \pm 0.107	1.221 \pm 0.380	1.129 \pm 0.363
DSB	0.953 \pm 0.140	0.862 \pm 0.023	1.079 \pm 0.117
Reg. CNF*	—	0.825 \pm —	—
T. Net*	—	0.848 \pm —	—

Table 4. Schrödinger bridge flow comparison, showing average error over flow time to ground truth averaged over 5 models for SB-CFM and 5 dynamics from DSB.

	SB-CFM	DSB
8gaussians	0.454 \pm 0.164	1.440 \pm 0.720
moon-8gaussians	1.377 \pm 0.229	2.407 \pm 1.025
moons	0.283 \pm 0.048	0.333 \pm 0.129
scurve	0.297 \pm 0.064	0.383 \pm 0.134

SB-CFM reproduces Schrödinger bridge flows. There are a number of methods which theoretically converge to a Schrödinger bridge between two datasets. In Table 4 we compare SB-CFM and the diffusion Schrödinger bridge (DSB) method introduced in De Bortoli et al. (2021) on the quality of the learnt Schrödinger bridges based on the average 2-Wasserstein distance to ground truth Schrödinger bridge samples over 18 time steps. Furthermore, SB-CFM is also significantly faster than DSB (Table S1).

6.2. Energy-based CFM

We show how CFM and OT-CFM can be adapted to the case where we do not have access to samples from the target distribution, but only an unnormalized density (equivalently, energy function) of the target, $R(x_1)$ (Figure 5). We consider the 10-dimensional funnel dataset from Hoffman & Gelman (2011). We aim to learn a flow from the 10-dimensional standard Gaussian to the energy function of the funnel. We consider two algorithms, each of which has certain advantages:

- (1) Reweighted importance sampling (RWIS): We construct a *weighted* batch of target points x_1 by sampling $x_1 \sim \mathcal{N}(\mathbf{0}, \mathbf{I})$ and assigning it a weight of $R(x_1)/\mathcal{N}(x_1; \mathbf{0}, \mathbf{I})$ normalized to sum to 1 over the

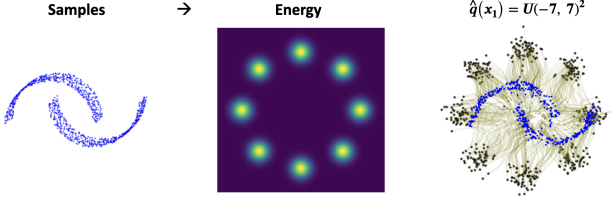


Figure 5. Flows (green) from (a) moons to (b) 8-Gaussians unnormalized density function learned using CFM with RWIS.

Table 5. Energy-based CFM results on the 10-dimensional funnel dataset: log-partition function estimation bias (mean and standard deviation over 10 runs) and time to generate 6000 samples from the trained ODE. With adaptive integration, OT-CFM requires fewer function evaluations. With a fixed-interval solver, OT-CFM has lower discretization error, leading to a better estimate. PIS baseline is from Zhang & Chen (2022).

	RWIS		MCMC	
	$\log \hat{Z}$	\int time	$\log \hat{Z}$	\int time
adaptive Dormand-Prince (tolerance 0.01) integration				
CFM	-0.068 ± 0.041	$26.6 \pm 8.4s$	0.029 ± 0.037	$34.6 \pm 6.0s$
OT-CFM	-0.076 ± 0.098	$13.3 \pm 1.7s$	0.009 ± 0.045	$12.8 \pm 1.2s$
FM	-0.033 ± 0.057	$26.5 \pm 7.7s$	0.027 ± 0.031	$30.9 \pm 5.8s$
Euler ($N = 10$) integration				
CFM	0.281 ± 0.202	$4.0 \pm 0.8s$	0.336 ± 0.030	$3.7 \pm 0.7s$
OT-CFM	-0.039 ± 0.030	$4.2 \pm 0.6s$	0.146 ± 0.107	$4.1 \pm 0.8s$
FM	0.176 ± 0.044	$4.1 \pm 0.7s$	0.334 ± 0.066	$3.9 \pm 0.6s$
Euler-Maruyama ($N = 100$) integration				
PIS (SDE)	-0.018 ± 0.020			

batch. The FM and CFM objectives handle weighted samples in a trivial way (by simply using the weights as $q(x_1)$ in Table 1), while OT-CFM treats the weights as target marginals in constructing the OT plan between x_0 and x_1 . We expect RWIS to perform well when batches are large and the proposal and target distributions are sufficiently similar; otherwise, numerical explosion of the importance weights can hinder learning.

- (2) MCMC: We use samples from a long-run Metropolis-adjusted Langevin MCMC chain on the target density as approximate target samples. We expect this method to perform well when the MCMC mixes well; otherwise, modes of the target density may be missed.

As an evaluation metric, we use the estimation bias of the log-partition function using a reweighted variational bound, following prior work that studied the problem using SDE modeling (Zhang & Chen, 2022). The computation of this metric for CNFs is given in the Appendix (§D.6).

The results are shown in Table 5. When an adaptive ODE integrator is used, all algorithms achieve similar results (no pair of mean log-partition function estimates is statistically distinguishable with $p < 0.1$ under a Welch’s t -test) but OT-CFM is about twice as efficient as CFM and FM. However, with a fixed computation budget for ODE integration, OT-CFM performs significantly better.

Table 6. Mean MMD between target and transformed source samples of CelebA latent vectors. Mean and standard deviation over 40 attributes and both translation directions ($- \leftrightarrow +$) for each attribute. ‘Identity’ refers to performing no translation and treating source samples as approximate samples from the target.

$\times 10^{-3}$	$\sigma = 0.1$	$\sigma = 0.3$	$\sigma = 1$
Identity	9.17 ± 5.68	9.17 ± 5.68	9.17 ± 5.68
CFM	4.85 ± 5.09	3.44 ± 2.03	1.59 ± 0.83
OT-CFM	2.81 ± 2.62	1.91 ± 1.30	1.04 ± 0.60

6.3. OT-CFM for Unsupervised Translation

We show how CFM can be used to learn a mapping between two unpaired datasets in high-dimensional space using the CelebA dataset (Liu et al., 2015; Sun et al., 2014), which consists of $\sim 200k$ images of faces together with 40 binary attribute annotations. For each attribute, we wish to learn an invertible mapping between images with and without the attribute (e.g., ‘not smiling’ \leftrightarrow ‘smiling’).

To reduce dimensionality, we first train a VAE on the images and encode them as 128-dimensional latent vectors. For each attribute, we learn a flow to map between the embeddings of images without the attribute and those of images with the attribute. After the flow is learned, we push forward a held-out set of negative vectors by the flow and compare them to the held-out positive vectors and vice versa. As a metric of divergence, we use maximum mean discrepancy (MMD) with a broad Gaussian kernel ($\exp(-\|x - y\|^2 / (2 \cdot 128))$).

The results aggregated over all attributes are shown in Table 6, showing that OT-CFM discovers a better mapping than other methods. Although MMD is lower for larger σ , we found that the alignment is less natural when σ is large, and performance begins to degrade when $\sigma > 1$. Figure S8 shows several visualizations of the learned trajectories.

Finally, while here we work in a latent space, future work should consider learning flows directly in image space, where GAN-based approaches (Zhu et al., 2017) continue to dominate.

7. Conclusion

We have introduced a novel simulation-free objective for learning continuous-time flows conditioned on a general source distribution. This can be seen as an alternative approach to training continuous normalizing flows and conditional flow models that does not require integration over time during training. Furthermore, we have shown that lifting the static optimal transport problem to the dynamic setting leads to more efficient training and inference of flow models by lowering variance of the objective and simplifying flows. One limitation of this work is that it requires closed-form

conditional flows. This limits its applicability to situations where we want to regularize the marginal flows based on prior information (Tong et al., 2020). We expect future work to overcome these limitations and hope that ideas from continuous flow matching will improve high-dimensional generative models.

Acknowledgments

We would like to thank Stefano Massaroli for productive conversations as well as thank Xinyu Yuan and Marco Jiralerspong for their helpful comments and feedback on the manuscript. The authors acknowledge funding from CIFAR, Genentech, Samsung, and IBM. In addition, K.F. acknowledges funding from NSERC (RGPIN-2019-06512) and G.W. acknowledges funding from NSERC Discovery grant 03267 and NIH grant R01GM135929.

References

- Alee, H., Theis, F. J., and Kilbertus, N. Beyond predictions in neural ODEs: Identification and interventions. *arXiv preprint 2106.12430*, 2021.
- Austin, J., Johnson, D. D., Ho, J., Tarlow, D., and van den Berg, R. Structured denoising diffusion models in discrete state-spaces. *Neural Information Processing Systems (NeurIPS)*, 2021.
- Bao, F., Li, C., Zhu, J., and Zhang, B. Analytic-dpm: An analytic estimate of the optimal reverse variance in diffusion probabilistic models. *International Conference on Learning Representations (ICLR)*, 2022.
- Ben-Hamu, H., Cohen, S., Bose, J., Amos, B., Grover, A., Nickel, M., Chen, R. T. Q., and Lipman, Y. Matching normalizing flows and probability paths on manifolds. *International Conference on Machine Learning (ICML)*, 2022.
- Bunne, C., Meng-Papaxanthos, L., Krause, A., and Cuturi, M. Proximal optimal transport modeling of population dynamics. *Artificial Intelligence and Statistics (AISTATS)*, 2022.
- Burkhardt, D., Bloom, J., Cannoodt, R., Luecken, M. D., Krishnaswamy, S., Lance, C., Pisco, A. O., and Theis, F. J. Multimodal single-cell integration across time, individuals, and batches. In *NeurIPS Competitions*, 2022.
- Chen, R. T. Q., Rubanova, Y., Bettencourt, J., and Duvenaud, D. Neural ordinary differential equations. *Neural Information Processing Systems (NeurIPS)*, 2018.
- Corso, G., Stärk, H., Jing, B., Barzilay, R., and Jaakkola, T. Diffdock: Diffusion steps, twists, and turns for molecular docking. *arXiv preprint 2210.01776*, 2022.
- Cuturi, M. Sinkhorn distances: Lightspeed computation of optimal transport. *Neural Information Processing Systems (NIPS)*, 2013.
- De Bortoli, V., Thornton, J., Heng, J., and Doucet, A. Diffusion schrödinger bridge with applications to score-based generative modeling. *Neural Information Processing Systems (NeurIPS)*, 2021.
- Dhariwal, P. and Nichol, A. Diffusion models beat gans on image synthesis. *Neural Information Processing Systems (NeurIPS)*, 2021.
- Fatras, K., Zine, Y., Flamary, R., Gribonval, R., and Courty, N. Learning with minibatch wasserstein: Asymptotic and gradient properties. *Artificial Intelligence and Statistics (AISTATS)*, 2020.
- Fatras, K., Séjourné, T., Courty, N., and Flamary, R. Unbalanced minibatch optimal transport; applications to domain adaptation. *International Conference on Machine Learning (ICML)*, 2021a.
- Fatras, K., Zine, Y., Majewski, S., Flamary, R., Gribonval, R., and Courty, N. Minibatch optimal transport distances; analysis and applications. *arXiv preprint 2101.01792*, 2021b.
- Finlay, C., Jacobsen, J.-H., Nurbekyan, L., and Oberman, A. M. How to train your neural ode: The world of jacobian and kinetic regularization. *International Conference on Machine Learning (ICML)*, 2020.
- Flamary, R., Courty, N., Gramfort, A., Alaya, M. Z., Boissunon, A., Chambon, S., Chapel, L., Corenflos, A., Fatras, K., Fournier, N., Gautheron, L., Gayraud, N. T. H., Janati, H., Rakotomamonjy, A., Redko, I., Rolet, A., Schutz, A., Seguy, V., Sutherland, D. J., Tavenard, R., Tong, A., and Vayer, T. POT: Python Optimal Transport. *Journal of Machine Learning Research (JMLR)*, 22, 2021.
- Goodfellow, I. J., Pouget-Abadie, J., Mirza, M., Xu, B., Warde-Farley, D., Ozair, S., Courville, A., and Bengio, Y. Generative adversarial nets. *Neural Information Processing Systems (NIPS)*, 2014.
- Grathwohl, W., Chen, R. T. Q., Bettencourt, J., Sutskever, I., and Duvenaud, D. Ffjord: Free-form continuous dynamics for scalable reversible generative models. *International Conference on Learning Representations (ICLR)*, 2019.
- Ho, J., Jain, A., and Abbeel, P. Denoising diffusion probabilistic models. *Neural Information Processing Systems (NeurIPS)*, 2020.
- Hoffman, M. D. and Gelman, A. The No-U-turn sampler: adaptively setting path lengths in Hamiltonian Monte Carlo. *Journal of Machine Learning Research (JMLR)*, 15:1593–1623, 2011.

- Huguet, G., Magruder, D. S., Tong, A., Fasina, O., Kuchroo, M., Wolf, G., and Krishnaswamy, S. Manifold interpolating optimal-transport flows for trajectory inference. *Neural Information Processing Systems (NeurIPS)*, 2022a.
- Huguet, G., Tong, A., Zapatero, M. R., Wolf, G., and Krishnaswamy, S. Geodesic Sinkhorn: Optimal transport for high-dimensional datasets. *arXiv preprint 2211.00805*, 2022b.
- Kingma, D. P. and Welling, M. Auto-encoding variational bayes. *International Conference on Learning Representations (ICLR)*, 2014.
- Klambauer, G., Unterthiner, T., Mayr, A., and Hochreiter, S. Self-normalizing neural networks. *Neural Information Processing Systems (NIPS)*, 2017.
- Lehmann, E. L. and Casella, G. *Theory of point estimation*. Springer Science & Business Media, 2006.
- Léonard, C. Some properties of path measures. In Donati-Martin, C., Lejay, A., and Rouault, A. (eds.), *Séminaire de Probabilités XLVI*, pp. 207–230. Springer, 2014a.
- Léonard, C. A survey of the schrödinger problem and some of its connections with optimal transport. *Discrete and Continuous Dynamical Systems*, 34(4):1533–1574, 2014b.
- Leygonie, J., She, J., Almahairi, A., Rajeswar, S., and Courville, A. Adversarial computation of optimal transport maps. *arXiv preprint 1906.09691*, 2019.
- Li, X., Wong, T.-K. L., Chen, R. T. Q., and Duvenaud, D. Scalable gradients for stochastic differential equations. *Artificial Intelligence and Statistics (AISTATS)*, 2020.
- Lipman, Y., Chen, R. T. Q., Ben-Hamu, H., Nickel, M., and Le, M. Flow matching for generative modeling. *arXiv preprint 2210.02747*, 2022.
- Liu, Z., Luo, P., Wang, X., and Tang, X. Deep learning face attributes in the wild. *International Conference on Computer Vision (ICCV)*, 2015.
- Loshchilov, I. and Hutter, F. Decoupled weight decay regularization. *International Conference on Learning Representations (ICLR)*, 2019.
- Lu, C., Zhou, Y., Bao, F., Chen, J., Li, C., and Zhu, J. Dpm-solver: A fast ode solver for diffusion probabilistic model sampling in around 10 steps. *Neural Information Processing Systems (NeurIPS)*, 2022.
- Makkuva, A. V., Taghvaei, A., Oh, S., and Lee, J. D. Optimal transport mapping via input convex neural networks. *International Conference on Machine Learning (ICML)*, 2020.
- Moon, K. R., van Dijk, D., Wang, Z., Gigante, S., Burkhardt, D. B., Chen, W. S., Yim, K., van den Elzen, A., Hirn, M. J., Coifman, R. R., Ivanova, N. B., Wolf, G., and Krishnaswamy, S. Visualizing structure and transitions in high-dimensional biological data. *Nat Biotechnol*, 37(12):1482–1492, 2019.
- Onken, D., Fung, S. W., Li, X., and Ruthotto, L. OT-Flow: Fast and accurate continuous normalizing flows via optimal transport. *Association for the Advancement of Artificial Intelligence (AAAI)*, 2021.
- Paszke, A., Gross, S., Massa, F., Lerer, A., Bradbury, J., Chanan, G., Killeen, T., Lin, Z., Gimelshein, N., Antiga, L., Desmaison, A., Kopf, A., Yang, E., DeVito, Z., Raison, M., Tejani, A., Chilamkurthy, S., Steiner, B., Fang, L., Bai, J., and Chintala, S. PyTorch: An Imperative Style, High-Performance Deep Learning Library. *Neural Information Processing Systems (NeurIPS)*, 2019.
- Peyré, G. and Cuturi, M. Computational optimal transport. *Foundations and Trends in Machine Learning*, 11(5-6): 355–607, 2019.
- Rezende, D. J. and Mohamed, S. Variational inference with normalizing flows. *International Conference on Machine Learning (ICML)*, 2015.
- Rozen, N., Grover, A., Nickel, M., and Lipman, Y. Moser flow: Divergence-based generative modeling on manifolds. *Neural Information Processing Systems (NeurIPS)*, 2021.
- Salimans, T. and Ho, J. Progressive distillation for fast sampling of diffusion models. *International Conference on Learning Representations (ICLR)*, 2022.
- Schiebinger, G., Shu, J., Tabaka, M., Cleary, B., Subramanian, V., Solomon, A., Gould, J., Liu, S., Lin, S., Berube, P., Lee, L., Chen, J., Brumbaugh, J., Rigollet, P., Hochedlinger, K., Jaenisch, R., Regev, A., and Lander, E. S. Optimal-transport analysis of single-cell gene expression identifies developmental trajectories in reprogramming. *Cell*, 176(4):928–943.e22, 2019.
- Schrödinger, E. Sur la théorie relativiste de l’électron et l’interprétation de la mécanique quantique. *Annales de l’Institut Henri Poincaré*, 2(4):269–310, 1932.
- Sohl-Dickstein, J., Weiss, E. A., Maheswaranathan, N., and Ganguli, S. Deep unsupervised learning using nonequilibrium thermodynamics. *International Conference on Machine Learning (ICML)*, 2015.
- Song, J., Meng, C., and Ermon, S. Denoising diffusion implicit models. *International Conference on Learning Representations (ICLR)*, 2021a.

- Song, Y. and Ermon, S. Generative modeling by estimating gradients of the data distribution. *Neural Information Processing Systems (NeurIPS)*, 2019.
- Song, Y. and Ermon, S. Improved techniques for training score-based generative models. *Neural Information Processing Systems (NeurIPS)*, 2020.
- Song, Y., Sohl-Dickstein, J., Kingma, D. P., Kumar, A., Ermon, S., and Poole, B. Score-based generative modeling through stochastic differential equations. *International Conference on Learning Representations (ICLR)*, 2021b.
- Sun, Y., Wang, X., and Tang, X. Deep learning face representation by joint identification-verification. *Neural Information Processing Systems (NIPS)*, 2014.
- Tong, A., Huang, J., Wolf, G., van Dijk, D., and Krishnaswamy, S. TrajectoryNet: A dynamic optimal transport network for modeling cellular dynamics. *International Conference on Machine Learning (ICML)*, 2020.
- Vargas, F., Thodoroff, P., Lawrence, N. D., and Lamacraft, A. Solving schrödinger bridges via maximum likelihood. *Entropy*, 23(9), 2021.
- Wang, G., Jiao, Y., Xu, Q., Wang, Y., and Yang, C. Deep generative learning via Schrödinger bridge. *International Conference on Machine Learning (ICML)*, 2021.
- Watson, D., Chan, W., Ho, J., and Norouzi, M. Learning fast samplers for diffusion models by differentiating through sample quality. *International Conference on Learning Representations (ICLR)*, 2022a.
- Watson, J. L., Juergens, D., Bennett, N. R., Trippe, B. L., Yim, J., Eisenach, H. E., Ahern, W., Borst, A. J., Ragotte, R. J., Milles, L. F., Wicky, B. I. M., Hanikel, N., Pellock, S. J., Courbet, A., Sheffler, W., Wang, J., Venkatesh, P., Sappington, I., Torres, S. V., Lauko, A., De Bortoli, V., Mathieu, E., Barzilay, R., Jaakkola, T. S., DiMaio, F., Baek, M., and Baker, D. Broadly applicable and accurate protein design by integrating structure prediction networks and diffusion generative models. *bioRxiv preprint 2022.12.09.519842*, 2022b.
- Yeo, G. H. T., Saksena, S. D., and Gifford, D. K. Generative modeling of single-cell time series with PRESCIENT enables prediction of cell trajectories with interventions. *Nat Commun*, 12(1):3222, 2021. ISSN 2041-1723. doi: 10.1038/s41467-021-23518-w.
- Zhang, Q. and Chen, Y. Path integral sampler: a stochastic control approach for sampling. *International Conference on Learning Representations (ICLR)*, 2022.
- Zhu, J.-Y., Park, T., Isola, P., and Efros, A. A. Unpaired image-to-image translation using cycle-consistent adversarial networks. *International Conference on Computer Vision (ICCV)*, 2017.

Supplementary Material

A. Proofs of Theorems

Theorem 3.1. *The marginal vector field (eq. 9) generates the marginal probability path (eq. 8) from $p_0(x)$ given any $q(z)$ independent of x and t .*

Proof of Theorem 3.1. To verify this, we first check that p_t and u_t satisfy the continuity equation.

We start with the derivative w.r.t. time of eq. 8

$$\frac{d}{dt}p_t(x) = \frac{d}{dt} \int p_t(x|z)q(z)dz$$

by Leibniz Rule,

$$= \int \frac{d}{dt} (p_t(x|z)q(z)) dz$$

since $u_t(\cdot|z)$ generates $p_t(\cdot|z)$,

$$= \int \operatorname{div} (u_t(x|z)p_t(x|z)q(z)) dz$$

by Leibniz Rule,

$$= -\operatorname{div} \left(\int u_t(x|z)p_t(x|z)q(z)dz \right)$$

Using eq. 9,

$$= -\operatorname{div} (u_t(x)p_t(x))$$

satisfying the continuity equation $\frac{d}{dt}p_t(x) + \operatorname{div} (u_t(x)p_t(x)) = 0$. \square

Theorem 3.2. *Assuming that $p_t(x) > 0$ for all $x \in \mathbb{R}^d$ and $t \in [0, 1]$ and $q(z)$ independent of x and t , then, up to a constant independent of θ , L_{CFM} and L_{FM} are equal. Hence,*

$$\nabla_{\theta} L_{FM}(\theta) = \nabla_{\theta} L_{CFM}(\theta) \quad (11)$$

Proof of Theorem 3.2. For this proof we need eq. 8, eq. 9 and the existence and exchange of many integrals. As in [Lipman et al. \(2022\)](#) we assume that q , $p_t(x|z)$ are decreasing to zero at sufficient speed as $\|x\| \rightarrow \infty$ and that u_t , v_t , $\nabla_{\theta} v_t$ are bounded.

$$\begin{aligned} \nabla_{\theta} \mathbb{E}_{p_t(x)} \|v_{\theta}(t, x) - u_t(x)\|^2 &= \nabla_{\theta} \mathbb{E}_{p_t(x)} (\|v_{\theta}(t, x)\|^2 - 2 \langle v_{\theta}(t, x), u_t(x) \rangle + \|u_t(x)\|^2) \\ &= \nabla_{\theta} \mathbb{E}_{p_t(x)} (\|v_{\theta}(t, x)\|^2 - 2 \langle v_{\theta}(t, x), u_t(x) \rangle) \\ \nabla_{\theta} \mathbb{E}_{q(z), p_t(x|z)} \|v_{\theta}(t, x) - u_t(x|z)\|^2 &= \\ \nabla_{\theta} \mathbb{E}_{q(z), p_t(x|z)} (\|v_{\theta}(t, x)\|^2 - 2 \langle v_{\theta}(t, x), u_t(x|z) \rangle + \|u_t(x|z)\|^2) &= \\ \mathbb{E}_{q(z), p_t(x|z)} \nabla_{\theta} (\|v_{\theta}(t, x)\|^2 - 2 \langle v_{\theta}(t, x), u_t(x|z) \rangle) & \end{aligned}$$

By bilinearity of the 2-norm and since u_t is independent of θ . Next,

$$\begin{aligned} \mathbb{E}_{p_t(x)} \|v_{\theta}(t, x)\|^2 &= \int \|v_{\theta}(t, x)\|^2 p_t(x) dx \\ &= \iint \|v_{\theta}(t, x)\|^2 p_t(x|z)q(z) dz dx \\ &= \mathbb{E}_{q(z), p_t(x|z)} \|v_{\theta}(t, x)\|^2 \end{aligned}$$

Finally,

$$\begin{aligned}
 \mathbb{E}_{p_t(x)} \langle v_\theta(t, x), u_t(x) \rangle &= \int \left\langle v_\theta(t, x), \frac{\int u_t(x|z) p_t(x|z) q(z) dz}{p_t(x)} \right\rangle p_t(x) dx \\
 &= \int \left\langle v_\theta(t, x), \int u_t(x|z) p_t(x|z) q(z) dz \right\rangle dx \\
 &= \iint \langle v_\theta(t, x), u_t(x|z) \rangle p_t(x|z) q(z) dz dx \\
 &= \mathbb{E}_{q(z), p_t(x|z)} \langle v_\theta(t, x), u_t(x|z) \rangle
 \end{aligned}$$

Where we first substitute eq. 9 then change the order of integration for the final equality. Since at all times t the gradients of L_{FM} and L_{CFM} are equal, $\nabla_\theta L_{FM}(\theta) = \nabla_\theta L_{CFM}(\theta)$ \square

Proposition 4.1. *The marginal p_t corresponding to $q(z)$, $p_t(x|z)$, and $u_t(x|z)$ in eqs. 14-16 has boundary conditions $p_1 = q_1 * \mathcal{N}(x | 0, \sigma^2)$ and $p_0 = q_0 * \mathcal{N}(x | 0, \sigma^2)$.*

Proof of Proposition 4.1. We start with eq. 8 to show the result of the lemma. We note that $q(z) = q((x_0, x_1)) = q(x_0)q(x_1)$

$$\begin{aligned}
 p_t(x) &= \int p_t(x|z) q(z) dz \\
 &= \int \mathcal{N}(x | tx_1 + (1-t)x_0, \sigma^2) q((x_0, x_1)) d(x_0, x_1) \\
 &= \iint \mathcal{N}(x | tx_1 + (1-t)x_0, \sigma^2) q(x_0) q(x_1) dx_0 dx_1
 \end{aligned}$$

evaluated at $i = 0, 1$ respectively. Therefore, at $t = 0$,

$$\begin{aligned}
 p_0(x) &= \iint \mathcal{N}(x | x_0, \sigma^2) q(x_0) q(x_1) dx_0 dx_1 \\
 &= \int \mathcal{N}(x | x_0, \sigma^2) q(x_0) dx_0 \\
 &= q(x_0) * \mathcal{N}(x | 0, \sigma^2).
 \end{aligned}$$

This is also true for $t = 1$. \square

Proposition 4.2. *The results of Prop. 4.1 also hold for $q(z)$ in eq. 17. Furthermore, as $\sigma^2 \rightarrow 0$ the marginal path p_t and field u_t are the unique minimizers of eq. 4, i.e., u_t solves the dynamic optimal transport problem between q_0 and q_1 .*

Proof of Proposition 4.2. Given π a 2-Wasserstein optimal transport map with marginals q_0 and q_1 , we have $\int \pi(x_0, x_1) dx_1 = q_0$ at $t = 0$ and $\int \pi(x_0, x_1) dx_0 = q_1$ at $t = 1$. Then,

$$\begin{aligned}
 p_t(x) &= \int \mathcal{N}(x | tx_1 + (1-t)x_0, \sigma^2) \pi(x_0, x_1) d(x_0, x_1) \\
 &= \iint \mathcal{N}(x | tx_1 + (1-t)x_0, \sigma^2) \pi(x_0, x_1) dx_0 dx_1
 \end{aligned}$$

Therefore, at $t = 0$,

$$\begin{aligned}
 p_0(x) &= \iint \mathcal{N}(x | x_0, \sigma^2) \pi(x_0, x_1) dx_0 dx_1 \\
 &= \int \mathcal{N}(x | x_0, \sigma^2) \left(\int \pi(x_0, x_1) dx_1 \right) dx_0 \\
 &= \int \mathcal{N}(x | x_0, \sigma^2) q(x_0) dx_0 \\
 &= q(x_0) * \mathcal{N}(x | 0, \sigma^2).
 \end{aligned}$$

This is also true for $t = 1$.

As for $\sigma^2 \rightarrow 0$, $p(x|z) = \delta_z(x)$, then $p_t(x) = \mathbb{E}_{p(z)}\delta_z(x)$, which implies the marginal path $u_t(x) = tx_1 + (1-t)x_0$ and do not cross each other, i.e., u_t solves the dynamic optimal transport problem between q_0 and q_1 . \square

Proposition 4.3. *The flow $u_t(x)$ defined by eq. 19 and eq. 21 generates the same marginal probability path as the solution π^* to the Schrödinger bridge problem in eq. 18.*

Proof of Proposition 4.3. Using Theorem 2.4 of Léonard (2014a), De Bortoli et al. (2021) showed that the initial and terminal marginals of π^* are the solution to the static OT problem

$$\pi^*(x_0, x_1) = \arg \min \text{KL}(\pi^*(x_0, x_1) \| p_{\text{ref}}(x_0, x_1)),$$

while the conditional path distributions $\pi^*(-|x_0, x_1)$ minimize $\mathbb{E}_{x_0, x_1 \sim \pi^*(x_0, x_1)} \text{KL}(\pi^*(-|x_0, x_1) \| p_{\text{ref}}(-|x_0, x_1))$.

The optimization problem for $\pi^*(x_0, x_1)$ is equivalent to the entropy-regularized optimal transport problem with optimum $\pi_{2\sigma^2}$, as observed by De Bortoli et al. (2021). (The key observation is that $\log p_{\text{ref}}(x_0, x_1) = \frac{c(x_0, x_1)^\alpha}{2\sigma^2} + \text{const.}$, where $c(x, y) = \|x - y\|$ and $\alpha = 2$.) The divergences between conditional path distributions are optimized by Brownian bridges with diffusion scale σ pinned at x_0 and x_1 , which are well-known to have marginal probability path p_t in eq. 20, and, by eq. 6, are generated by the vector fields u_t in eq. 21. \square

Proposition A.1. *For any $\sigma \in \mathbb{R}_+$ source conditional flow matching has an equivalent marginal probability flow $p_t(x)$ to Lipman et al. (2022) flow matching.*

Proof. To prove the proposition, we use the fact that the Gaussian family can be generated by location-scale transformations (see e.g. Lehmann & Casella, 2006), i.e. we can express any Gaussian $Z_0 \sim \mathcal{N}(\mu_0, \sigma_0^2)$ as $Z_0 = \mu_0 + \sigma_0 Z$ where $Z \sim \mathcal{N}(0, 1)$. Recall that the density $p_t(x)$ has the form $p_t(x) = \int p_t(x|z)q(z)dz$, to show the equivalence between the flow from FM and source conditional flow matching, we have to show that $p_t(x|x_1)$ is the same for both methods, that is we show that CFM with variance $(\sigma t)^2 + 2\sigma t(1-t)$ is equivalent to FM with variance $(t\sigma - t + 1)^2$ (Def. 12). Since $p_t(x|x_0, x_1)$ is $\mathcal{N}(tx_1 + (1-t)x_0, \sigma t(\sigma t - 2t + 2))$ we can write the random variable $X|X_0, X_1$ as

$$X|X_0, X_1 = tx_1 + (1-t)x_0 + (\sigma t(\sigma t - 2t + 2))^{1/2} Z,$$

where $Z \sim \mathcal{N}(0, 1)$. Without conditioning on X_0 , we have

$$X|X_1 = tx_1 + (1-t)X_0 + (\sigma t(\sigma t - 2t + 2))^{1/2} Z.$$

By assumption $X_0 \sim \mathcal{N}(0, 1)$, thus $X|X_1$ is Gaussian, since a linear transformation of Gaussian distributions is also Gaussian. To define its distribution, we only have to define its expectation and variance. By linearity of expectation, we find $\mathbb{E}(X|X_1) = tx_1$, and by independence of X_0 and Z we have

$$\begin{aligned} \text{Var}(X|X_1) &= (1-t)^2 \text{Var}(X_0) + (\sigma t(\sigma t - 2t + 2)) \text{Var}(Z) \\ &= (1-t)^2 + (\sigma t(\sigma t - 2t + 2)) = (t\sigma - t + 1)^2, \end{aligned}$$

hence the flow from source conditional flow matching is the same as FM. \square

Proposition A.2. *If π is a Monge map, the objective variance of OT-CFM goes to zero as $\sigma \rightarrow 0$, i.e.,*

$$\mathbb{E}_{q(z)} \|u_t(x|z) - u_t(x)\|^2 \rightarrow 0 \text{ as } \sigma \rightarrow 0$$

for $u_t(x|z)$ in eq. 16.

Proof. This follows from a basic fact about the transport plan π . Specifically, that as $\sigma \rightarrow 0$, $D_{\text{KL}}(p_t(x|z^i) \| p_t(x|z^j)) \rightarrow \infty$ for an t, x for two distinct z^i, z^j . This means that $p_t(x|z) = p_t(x)$ for any t, x, z therefore

$$\begin{aligned} u_t(x) &= \mathbb{E}_{q(z)} u_t(x|z) p_t(x|z) / p_t(x) \\ &= u_t(x|z) \end{aligned}$$

\square

Proposition A.3. *The conditional vector field $u_t(x|\bar{z})$ defined by 24 converges to marginal vector field $u_t(x)$ defined by 9 as m goes to population size, i.e.,*

$$\|u_t(x|\bar{z}) - u_t(x)\|^2 \rightarrow 0$$

as $m \rightarrow |\mathcal{X}|$.

Proof. As $|z| \rightarrow |\mathcal{X}|$, by definition,

$$\begin{aligned} u_t(x|\bar{z}) &= \frac{\sum_i^m u_t(x|z^i) p_t(x|z^i) q(z^i)}{\sum_i^m p_t(x|z^i) q(z^i)} \\ &= \frac{\sum_{z \in \mathcal{X}} u_t(x|z) p_t(x|z) q(z)}{\sum_{z \in \mathcal{X}} p_t(x|z) q(z)} \\ &= \mathbb{E}_{q(z)} \frac{u_t(x|z) p_t(x|z)}{p_t(x)} \\ &= u_t(x) \end{aligned}$$

□

B. Algorithm

In Algorithm 1 we presented the general algorithm for conditional flow matching given $q(z)$, $p_t(x|z)$, $u_t(x|z)$. In Table 1 we presented a number of settings of these leading to interesting probability paths. In practice, we may wish to compute $q(z)$ on the fly. Therefore in Algorithms 2, 3, and 4, we give algorithms for the simplified conditional flow matching, and minibatch versions of OT conditional flow matching and Schrödinger bridge conditional flow matching. In general these consist of first sampling a batch of data from both the source and the target empirical distributions, then resampling pairs of data either randomly (CFM) or according to some OT plan, (OT-CFM and SB-CFM).

B.1. Variance Reduction by Averaging Across Batches

As discussed in §4.5, and formalized in Proposition A.3 we can reduce variance in the target by averaging over multiple datapoints. Specifically, in this case we let $\bar{z} := \{z^i := (x_0^i, x_1^i)\}_{i=1}^m$, where z^i are i.i.d. from $q(z)$ and

$$p_t(x|\bar{z}) = \frac{\sum_i^m p_t(x|z^i) q(z^i)}{\sum_i^m q(z^i)} \quad (23)$$

$$u_t(x|\bar{z}) = \frac{\sum_i^m u_t(x|z^i) p_t(x|z^i) q(z^i)}{p_t(x|\bar{z})} \quad (24)$$

It takes roughly m times as long to compute the conditional target $u_t(x|\bar{z})$ but reduces the variance. As the evaluation and backpropagation through v_θ gets more difficult this tradeoff can be beneficial.

B.2. Modeling Energy Functions

If we have access to an energy function two (unnormalized) energy functions $\mathcal{R}_{\{0,1\}} : \mathcal{X} \rightarrow \mathbb{R}^+$ at the endpoints instead of i.i.d. samples $\mathbf{X}_t \sim q_t(x_t)$, then the objective must be slightly modified. We formulate the Energy Conditional Flow Matching Objective as

$$L_{ECFM} = \mathbb{E}_{t, \hat{q}_0(x_0), \hat{q}_1(x_1), p_t(x|x_0, x_1)} \left[\frac{R_0(x_0) R_1(x_1)}{\hat{q}_0(x_0) \hat{q}_1(x_1)} \|v_\theta(t, x) - u_t(x|x_0, x_1)\|_2^2 \right] \quad (25)$$

We can use this object to train a flow which matches the energies without access to samples. This is formalized in the following theorem.

Proposition B.1. *Assuming that $\hat{q}_{\{0,1\}}(x), p_t(x) > 0$ for all $x \in \mathcal{X}$ and $t \in [0, 1]$ then the gradients of L_{FM} and L_{ECFM} with respect to θ are equal up to some multiplicative constant c .*

$$\nabla_\theta L_{FM}(\theta) = c \nabla_\theta L_{ECFM}(\theta) \quad (26)$$

Algorithm 2 Simplified Conditional Flow Matching

Input: Sample-able distributions $\mathbf{X}_0, \mathbf{X}_1$, bandwidth σ , batchsize b , initial network v_θ .

while Training **do**

/ Sample batches of size b i.i.d. from the datasets */*

$\mathbf{x}_0 \sim \mathbf{X}_0; \quad \mathbf{x}_1 \sim \mathbf{X}_1$

$t \sim \mathcal{U}(0, 1)$

$\mu_t \leftarrow t\mathbf{x}_1 + (1-t)\mathbf{x}_0$

$\mathbf{x} \sim \mathcal{N}(\mu_t, \sigma^2 I)$

$L_{CFM}(\theta) \leftarrow \|v_\theta(t, \mathbf{x}) - (\mathbf{x}_1 - \mathbf{x}_0)\|^2$

$\theta \leftarrow \text{Update}(\theta, \nabla_\theta L_{CFM}(\theta))$

return v_θ

Algorithm 3 Minibatch OT Conditional Flow Matching

Input: Sample-able distributions $\mathbf{X}_0, \mathbf{X}_1$, bandwidth σ , batch size b , initial network v_θ .

while Training **do**

/ Sample batches of size b i.i.d. from the datasets */*

$\mathbf{x}_0 \sim \mathbf{X}_0; \quad \mathbf{x}_1 \sim \mathbf{X}_1$

$\pi \leftarrow \text{OT}(\mathbf{x}_1, \mathbf{x}_0)$

$(\mathbf{x}_0, \mathbf{x}_1) \sim \pi$

$t \sim \mathcal{U}(0, 1)$

$\mu_t \leftarrow t\mathbf{x}_1 + (1-t)\mathbf{x}_0$

$\mathbf{x} \sim \mathcal{N}(\mu_t, \sigma^2 I)$

$L_{CFM}(\theta) \leftarrow \|v_\theta(t, \mathbf{x}) - (\mathbf{x}_1 - \mathbf{x}_0)\|^2$

$\theta \leftarrow \text{Update}(\theta, \nabla_\theta L_{CFM}(\theta))$

return v_θ

Proof. Let $z_0 = \int_{\mathcal{X}} R_0(x)dx$, and $z_1 = \int_{\mathcal{X}} R_1(x)dx$ then $q(x_0) = \mathcal{R}_0(x_0)/z_0$, similarly $q(x_1) = \mathcal{R}_1(x_1)/z_1$, then

$$L_{ECFM}(\theta) = \mathbb{E}_{t, \hat{q}_0(x_0), \hat{q}_1(x_1), p_t(x|x_0, x_1)} \left[\frac{\mathcal{R}_0(x_0)\mathcal{R}_1(x_1)}{\hat{q}_0(x_0)\hat{q}_1(x_1)} \|v_\theta(t, x) - u_t(x|x_0, x_1)\|_2^2 \right] \quad (27)$$

$$= z_0 z_1 \mathbb{E}_{t, \hat{q}_0(x_0), \hat{q}_1(x_1), p_t(x|x_0, x_1)} \left[\frac{q_0(x_0)q_1(x_1)}{\hat{q}_0(x_0)\hat{q}_1(x_1)} \|v_\theta(t, x) - u_t(x|x_0, x_1)\|_2^2 \right] \quad (28)$$

$$= z_0 z_1 \int_{t, x_0, x_1, x} \left[q_0(x_0)q_1(x_1) \|v_\theta(t, x) - u_t(x|x_0, x_1)\|_2^2 \right] p_t(x|x_0, x_1) dx_0 dx_1 dx \quad (29)$$

$$= z_0 z_1 L_{CFM}(\theta) \quad (30)$$

where we use substitution for the first step and change the order of integration in the last step. With an application of [Theorem 3.2](#) the gradients are equivalent up to a factor of $z_0 z_1$ which does not depend on x . \square

Of course L_{ECFM} leaves the question of sampling open for high-dimensional spaces. Sampling uniformly does not scale well to high dimensions, so for practical reasons we may want a different sampling strategy.

We use this objective in [Figure 5](#) with a uniform proposal distribution as a toy example of this type of training.

C. Additional Results

We start this section by the definition of the entropy regularized OT problem:

$$W(q_0, q_1)_{2, \lambda}^2 = \inf_{\pi \in \Pi} \int_{\mathcal{X}^2} c(x, y)^2 \pi_\lambda(dx, dy) - \lambda H(\pi), \quad (31)$$

where $\lambda \in \mathbb{R}^+$ and $H(\pi) = \int \ln \pi(x, y) d\pi(dx, dy)$.

Algorithm 4 Minibatch Schrödinger Bridge Conditional Flow Matching

Input: Sample-able distributions $\mathbf{X}_0, \mathbf{X}_1$, bandwidth σ , batch size b , initial network v_θ .

while Training **do**

/* Sample batches of size b i.i.d. from the datasets */

$\mathbf{x}_0 \sim \mathbf{X}_0; \quad \mathbf{x}_1 \sim \mathbf{X}_1$

$\pi_{2\sigma^2} \leftarrow \text{Sinkhorn}(\mathbf{x}_1, \mathbf{x}_0, 2\sigma^2)$

$(\mathbf{x}_0, \mathbf{x}_1) \sim \pi_{2\sigma^2}$

$\mathbf{t} \sim \mathcal{U}(0, 1)$

$\mu_t \leftarrow \mathbf{t}\mathbf{x}_1 + (1 - \mathbf{t})\mathbf{x}_0$

$\mathbf{x} \sim \mathcal{N}(\mu_t, \sigma^2 \mathbf{t}(1 - \mathbf{t})\mathbf{I})$

$\mathbf{u}_t(\mathbf{x}|\mathbf{z}) \leftarrow \frac{1-2\mathbf{t}}{2\mathbf{t}(1-\mathbf{t})}(\mathbf{x} - (\mathbf{t}\mathbf{x}_1 + (1 - \mathbf{t})\mathbf{x}_0)) + (\mathbf{x}_1 - \mathbf{x}_0)$ \triangleright From eq. 21

$L_{CFM}(\theta) \leftarrow \|v_\theta(\mathbf{t}, \mathbf{x}) - \mathbf{u}_t(\mathbf{x}|\mathbf{z})\|^2$

$\theta \leftarrow \text{Update}(\theta, \nabla_\theta L_{CFM}(\theta))$

return v_θ

Regularized CNF tuning Continuous normalizing flows with a path length penalty optimize a relaxed form of a dynamic optimal transport problem (Tong et al., 2020; Finlay et al., 2020; Onken et al., 2021). Where dynamic optimal transport solves for the optimal vector field in terms of average path length where the marginals at time $t = 0$ and $t = 1$ are constrained to equal two input marginals q_0 and q_1 . Instead of this pair of hard constraints, regularized CNFs instead set $q_0 := \mathcal{N}(x | 0, 1)$ and optimize a loss of the form

$$L(x(t)) = -\log p(x(t)) + \lambda_e \int_0^1 \|v_\theta(t, x(t))\|^2 dt \quad (32)$$

where $\frac{dx}{dt} = v_\theta(t, x(t))$ and $\log p(x(T))$ is defined as

$$\log p(x(T)) = p(x(0)) + \int_0^T \frac{\partial \log p(x(t))}{\partial t} dt = p(x(0)) + \int_0^T -\text{tr} \left(\frac{dv_\theta}{dx(t)} \right) dt \quad (33)$$

where the second equality follows from the instantaneous change of variables theorem (Chen et al., 2018, Theorem 1). In practice it is difficult to pick a λ_e which both produces flows with short paths and allows the model to fit the data well. We analyze the effect of this parameter over three datasets in Figure S1. In this figure we analyze the Normalized 2-Wasserstein to the target distribution (which approaches 1 with good fit), and the Normalized Path Energy (NPE). We find a tradeoff between short paths (Low NPE) and good fit (Low 2-Wasserstein). We choose $\lambda_e = 0.1$ as a good tradeoff across datasets, which has paths that are not too much longer than optimal but also fits the data well.

Ablation results on batch size. Since we use Minibatch-OT for OT-CFM, when the minibatch size is equal to one, then OT-CFM is equivalent to CFM. This effect can be seen in Figure S2, where over four datasets, OT-CFM starts with equal path length and approximately equal 2-Wasserstein. Then the normalized path energy decreases surprisingly quickly plateauing after batchsize reaches ~ 64 . While the minibatch size needed to approximate the true dynamic optimal transport paths will vary with dataset (for example in the moon-8gaussian case we need a larger batch size) it is still somewhat surprising that such small batches are needed as this is less than 0.5% of the entire 10k point dataset per batch.

The effect of σ on fit and path length. Next we consider σ , the bandwidth parameter of the Gaussian conditional probability path. In Figure S3 we study the effect of σ on the fit (top) and the path energy (bottom). With $\sigma > 1$ methods start to underfit with high 2-Wasserstein error and either very long or very short paths. As for specific models, SB-CFM becomes unstable with σ too small due to the lack of convergence for the static Sinkhorn optimization with small regularization. FM and CFM follow similar trends where they fit fairly well with $\sigma \leq 1$ but have paths that are significantly longer than optimal by 2-3x. OT-CFM maintains near optimal path energies and near optimal fit until $\sigma > 1$.

Objective variance. Variance in the conditional objective target $u_t(x|z)$ varies across models. In Figure S4 we study the objective variance across CFM objective functions. Here we estimate the objective variance in eq. 22 as

$$\mathbb{E}_{x,t,z} \|u_t(x|z) - v_\theta(t, x)\|^2 \quad (34)$$

after training has converged. After training has converged v_θ should be very close to $u_t(x)$ so we use it as an empirical estimator of $u_t(x)$ to compute the variance. We find that across all datasets OT-CFM and SB-CFM have at least an order of

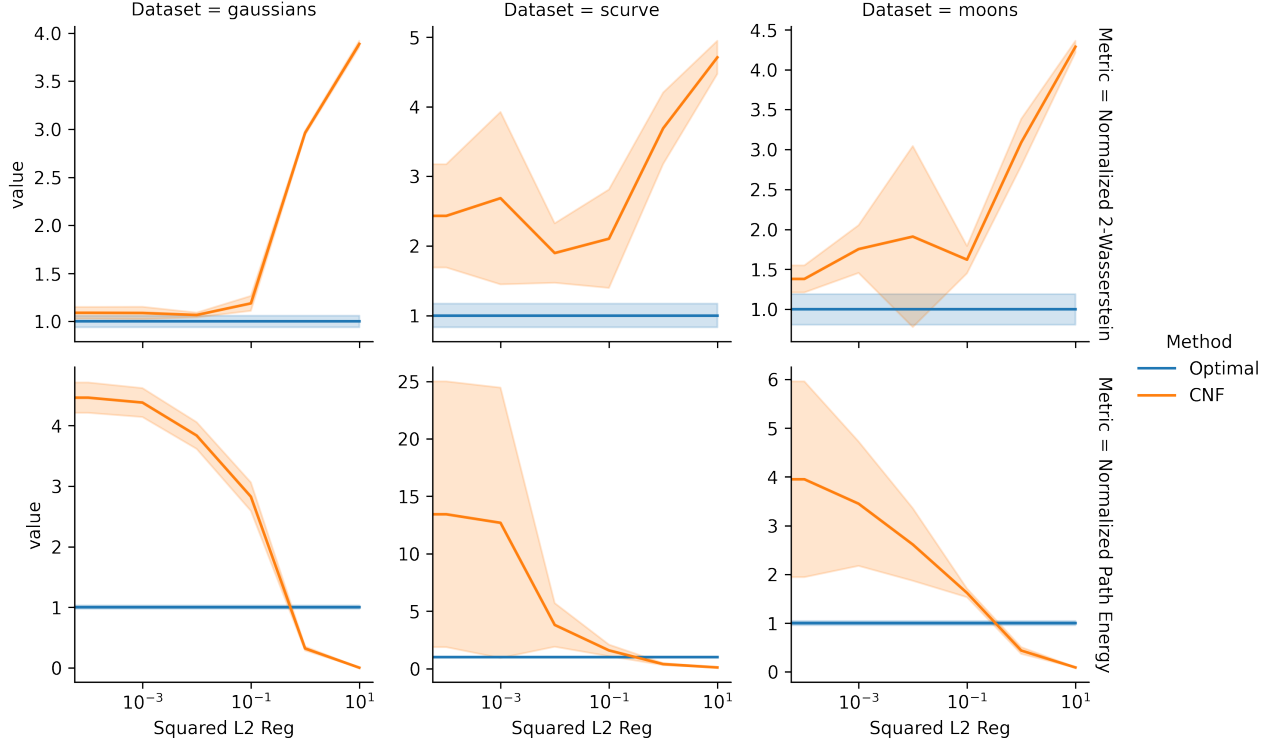


Figure S1. Evaluation of regularization strength of λ_e over 6 seeds in the range $[0, 10^{-5}, 10^2]$. $\lambda_e = 0.1$ performs the best in terms of minimizing path length and test error. We call this model "Regularized CNF".

magnitude lower variance than CFM and FM objectives. This correlates with faster training as measured by lower validation error in fewer steps for lower variance models as seen in Figure 3.

We examine the objective variance OV by conditioning $u_t(x|\mathbf{z})$ on a batch of pairs of data points, $\bar{\mathbf{z}} := \{z^i := (x_0^i, x_1^i)\}_{i=1}^m$, we can reduce the variance of the OV objective to 0 for all models as batchsize goes to population size. For the batchsize m range from 1 to the number of the population, we uniformly sample m pairs of points z^i and compute the probability $p_t(x|\bar{\mathbf{z}})$ and the objective $u_t(x|\bar{\mathbf{z}})$ from equation 23 and 24.

We also find that averaging over batches makes the network achieve a lower validation error in fewer steps and in less walltime Figure S5

Schrödinger bridge fit over simulation time. In Figure S7 we compare the fit of Diffusion Schrödinger Bridge model with SB-CFM conditioned on time. The Diffusion Schrödinger Bridge seems to outperform SB-CFM early in the trajectory, however fails to fit the bridge after many integration steps.

D. Experiment and Implementation Details

D.1. Physical Experimental Setup

All experiments were performed on a shared heterogenous high-performance-computing cluster. This cluster is primarily composed of GPU nodes with RTX8000, A100, and V100 Nvidia GPUs. Since the network and nodes are shared, other users may cause high variance in the training times of models. However, we believe that the striking difference between the convergence times in Table S1 and combined with the CFM training setup with a single CPU and the baseline models trained with two CPUs and a GPU, paints a clear picture as to how efficient CFM training is. Qualitatively, we feel that most CFMs converge quite a bit more rapidly than these metrics would suggest, often converging to a near optimal validation performance in minutes.

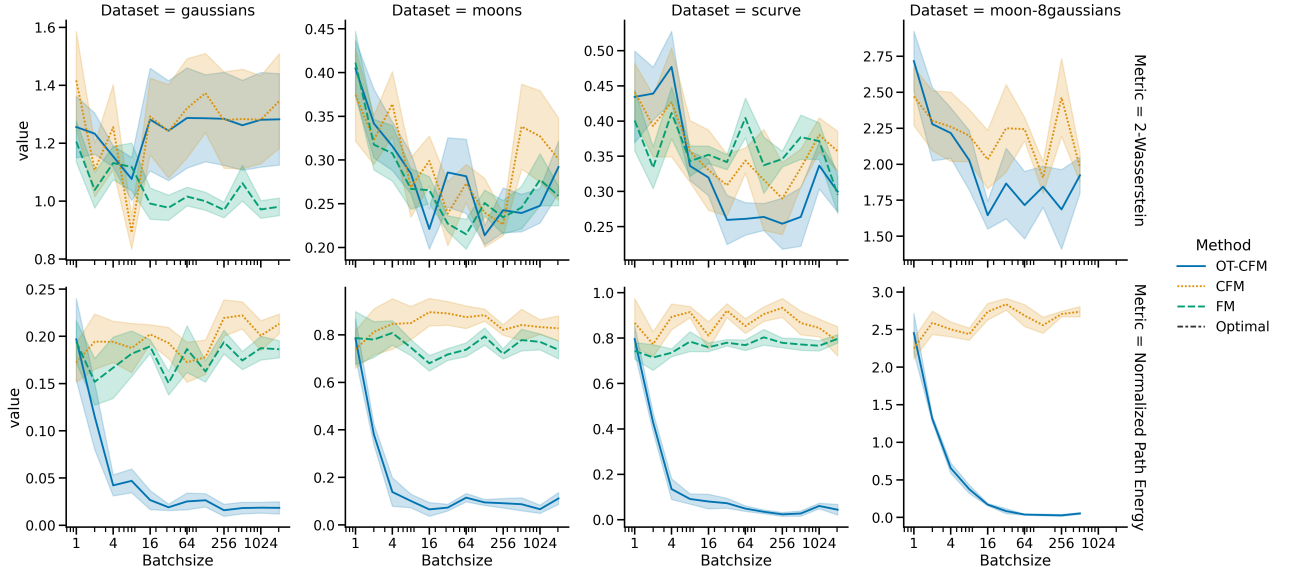


Figure S2. $\mu \pm \sigma$ of mean path length prediction error over 5 seeds. Lower is better. Introducing OT to CFM batches straightens paths lowering cost towards the optimal W^2 as compared to a standard random conditional flow matching network over all batch sizes.

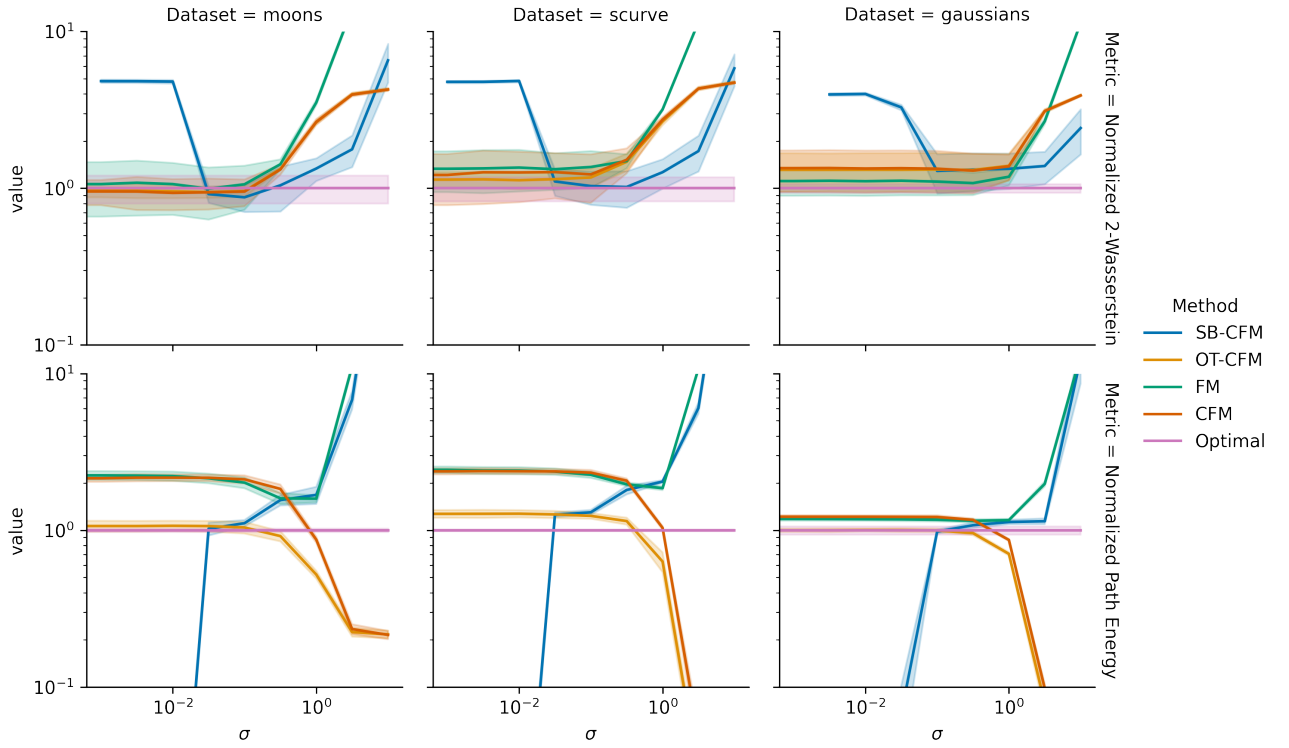


Figure S3. Evaluation of the effect of σ for conditional flow matching models. When $\sigma < 1$ OT-CFM

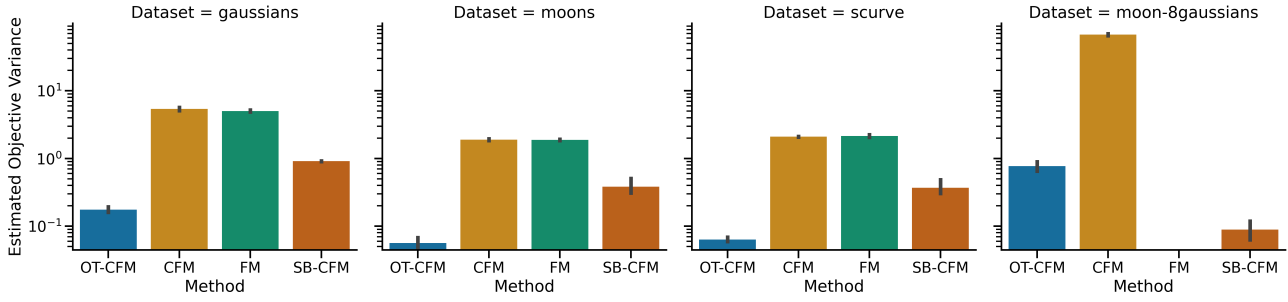


Figure S4. Estimated Objective Variance Eq. 22 for different methods with batch size 512, $\sigma = 0.1$ across datasets. OT-CFM and SB-CFM have significantly lower objective variance than CFM and FM which have roughly equivalent objective variance.

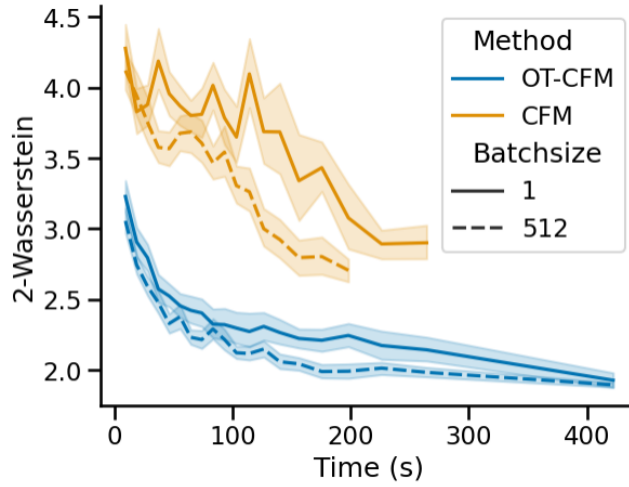


Figure S5. Validation 2-Wasserstein distance against training time with variance reduction by aggregation either with no aggregation (Batchsize 1) or aggregation over a minibatch (Batchsize 512). Variance reduction leads to faster training, especially for CFM where the objective variance is naturally larger than OT-CFM which sees a small performance gain.

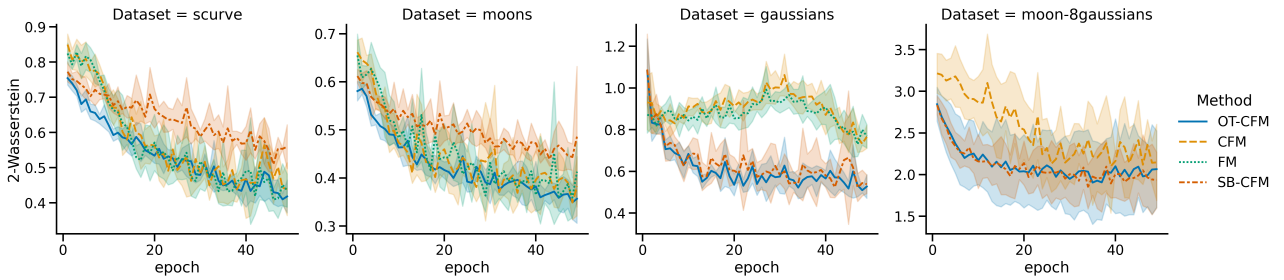


Figure S6. Extended results from Figure 3 over two more datasets. OT-CFM is still consistently the fastest converging method.

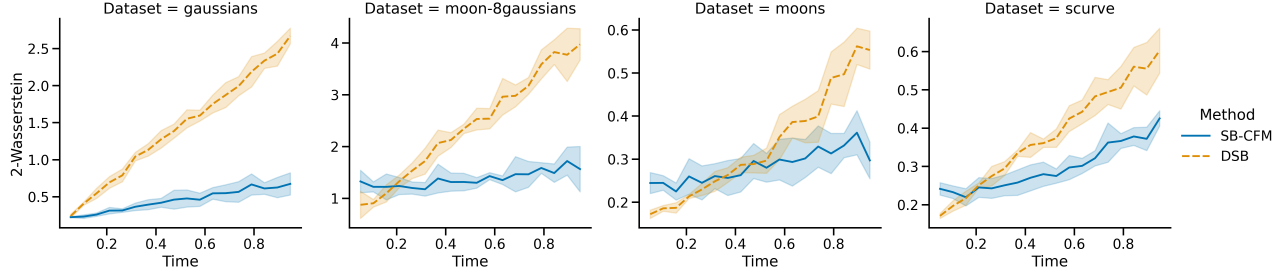


Figure S7. 2-Wasserstein Error between trajectories and ground truth Schrödinger Bridge samples over simulation time.

Table S1. Mean training time till convergence in 10^3 seconds over 5 seeds, with the exception of DSB, trained over 1 seed. CFM variants and DSB are trained on a single CPU with 5GB of memory where other baselines are given two CPUs and one GPU. CFM, with significantly fewer resources, still trains the fastest.

	8gaussians	moons-8gaussians	moons	scurve	mean
OT-CFM	1.284 ± 0.028	1.587 ± 0.204	1.464 ± 0.158	1.499 ± 0.157	1.484 ± 0.192
CFM	0.993 ± 0.021	1.102 ± 0.171	1.059 ± 0.158	1.008 ± 0.106	1.046 ± 0.132
FM	0.839 ± 0.096	—	1.076 ± 0.126	1.127 ± 0.123	1.014 ± 0.170
SB-CFM	0.713 ± 0.386	0.794 ± 0.293	1.143 ± 0.389	1.230 ± 0.424	0.935 ± 0.397
Reg. CNF	2.684 ± 0.052	—	9.154 ± 1.535	9.022 ± 3.207	8.021 ± 3.288
CNF	1.512 ± 0.234	—	17.124 ± 4.398	27.416 ± 13.299	18.810 ± 12.677
ICNN	3.712 ± 0.091	3.046 ± 0.496	2.558 ± 0.390	2.200 ± 0.034	2.912 ± 0.626
DSB	$5.418 \pm —$	$5.682 \pm —$	$5.428 \pm —$	$5.560 \pm —$	$5.522 \pm —$

D.2. 2D, Single-cell, and Schrödinger Bridge Experimental Setup

For all experiments we use the same architecture implemented in PyTorch (Paszke et al., 2019). We concatenate the flattened input $x \in \mathbb{R}^d$ and the time t as the $d + 1$ inputs to a network with three hidden layers of width 64 interspersed with SELU activations (Klambauer et al., 2017) followed by a linear output layer of width d . This forms our v_θ for all experiments. For all 2D and single-cell experiments we train for 1000 epochs and implement early stopping on the validation loss which checks the loss on a validation set every 10 epochs and stops training if there is no improvement for 30 epochs. We also set a time limit of 100 minutes for each CFM model. This is hit almost exclusively for SB-CFM models with small σ which are unstable to train due to instabilities and non-convergence of the Sinkhorn (Cuturi, 2013) transport plan optimization. We use the AdamW (Loshchilov & Hutter, 2019) optimizer with weight decay 10^{-5} with batchsize 512 by default in 2D experiments and 128 in the single cell datasets. For OT-CFM and SB-CFM we use exact linear programming EMD and Sinkhorn algorithms from the python optimal transport package (Flamary et al., 2021) For evaluation of trajectories unless otherwise noted we use the Runge-Kutta45 (rk4) ODE solver with 101 timesteps from 0 to 1.

D.3. Variance Reduction by Averaging

We tackle the exploration of the effects of reducing variance of the target $u_t(x|z)$ from two directions. The first is for small example where we can compute the ground truth $u_t(x)$ quickly, and the second is in the setting of trained models where we can estimate $u_t(x)$ with $v_\theta(t, x)$ after v_θ has converged.

We first consider the convergence of each flow matching objective (OT-CFM, CFM, FM, SB-CFM) to zero as a function of the batch size relative to the dataset size. This is done by first sampling t, x, z then computing the true objective variance across many samples. This appears in Figure 2.

We next consider the effect of averaging over a batch to reduce the variance of the objective in Figure 2 (right). Here Batchsize refers to the size of the batch we are averaging over. We aggregate this into a single target so that the model sees a single d dimensional target vector for one sampled x, t . This means that we can compare different aggregation sizes fairly.

D.4. Schrödinger Bridge Evaluation Setup

To evaluate how well Schrödinger Bridge models actually model a Schrödinger Bridge, we constrain ourselves to a small example with 1000 points. For any time t we can sample from the ground truth Schrödinger bridge density $p_t(x)$ as

$$(x_0, x_1) \sim \pi_{2\sigma^2}$$

$$X_t \sim \mathcal{N}(x \mid tx_1 + (1-t)x_0, \sigma t(1-t))$$

We sample trajectories of length 20 from $t = 0$ to $t = 1$ by integrating over time from $t = 0$ to $t = 1$. At each of the 18 intermediate timepoints we compute the 2-Wasserstein distance between a sample of size 1000 from the trajectories at that time and the ground truth X_t as above at that time. We reported the average across the 18 intermediate timepoints in Table 4 and plot the 2-Wasserstein distance over time in Figure S7.

SB-CFM Model We train SB-CFM with $\sigma = 1$ and batchsize=512 for each of the datasets. We save 1000 trajectories from a test set integrated with the tsit5 solver with atol=rtol=1e-4.

Diffusion Schrödinger bridge model implementation details We use the implementation from De Bortoli et al. (2021). Only the networks were changed for a fair comparison with CFM. The forward and backward networks are composed of an MLP with three hidden layers of size 64, with SELU activations in between layers. We used a time and a positional encoders composed of two layers of size 16 and 32 with LeakyReLU activations has inputs to the score network. The architectures are the same for the 2D examples and the single-cell examples (except for the input dimension). During training, we set the variance (γ in the author’s code) to 0.001 and did 20 steps to discretize the Langevin dynamic. We trained for 10k iterations with 10k particles and batch size of 512, for 20 iterative proportional fitting steps, and a learning rate set to 0.0001. For the interpolation task we used the tenth timepoint from the Langevin dynamic with the backward network trained to go from the distribution at time $t - 1$ to $t + 1$. All trajectories are evaluated from the backward dynamic. We use $\sigma = 1$ and batchsize=512.

D.5. Single-Cell Experimental Setup

We strove to be consistent with the experimental setup of Tong et al. (2020). For the Embryoid body (EB) data, we use the same processed artifact which contains the first 100 principle components of the data. For our tests we truncate to the first five dimensions, then whiten (subtract mean and divide by standard deviation) each dimension. For the Embryoid body (EB) dataset which consists of 5 timepoints collected over 30 days we train separate models leaving out times 1, 2, 3 in turn. We train a CFM over the full time scale (0-4). During testing we push forward all points X_{t-1} to time t as a distribution to test against.

For the Cite and Multi datasets these are sourced from the Multimodal Single-cell Integration challenge at NeurIPS 2022, a NeurIPS challenge hosted on Kaggle where the task was multi-modal prediction (Burkhardt et al., 2022). In this competition they used this data to investigate the predictability of RNA from chromatin accessibility and protein expression from RNA. Here, we repurpose this data for the task of time series interpolation. Both of these datasets consist of four timepoints from CD34+ hematopoietic stem and progenitor cells (HSPCs) collected on days 2, 3, 4, and 7. For more information and the raw data see the competition site.³ We preprocess this data slightly to remove patient specific effects by focusing on a single donor (donor 13176), then we again compute the first five principle components and again whiten each dimension to further normalize the data.

D.6. Energy-Based CFM

The 10-dimensional funnel dataset is defined by $\mathbf{x}_0 \sim \mathcal{N}(0, 1)$, $\mathbf{x}_{1,\dots,9} \sim \mathcal{N}(0, \exp(\mathbf{x}_0)\mathbf{I})$. We attempted to mimic the SDE model architecture from Zhang & Chen (2022) for the flow model $v_\theta(t, x)$. The time step t is encoded with 128-dimensional Fourier features, then both x and t are independently processed with two-layer MLPs. The two representations are concatenated and processed through another three-layer MLP to make the prediction. All MLPs use GELU activation and have 128 units per hidden layer. We trained all models with $\sigma = 0.05$ and learning rate 10^{-2} , the highest at which they were table, for 1500 batches of size 300, to be consistent with the settings from Zhang & Chen (2022).

³<https://www.kaggle.com/competitions/open-problems-multimodal/data>

The importance-weighted estimate of the log-partition function is defined

$$\log \hat{Z} = \log \frac{1}{K} \sum_{i=1}^K \frac{R(x_1^{(i)})}{\mathcal{N}(x_0^{(i)}; 0, \mathbf{I})} \left| \frac{\partial x_1}{\partial x_0} \right|_{x_0=x_0^{(i)}},$$

where $x_0^{(i)}$ are independent samples from the source distribution and $x_1^{(i)}$ is $x_0^{(i)}$ pushed forward by the flow (note that the Jacobian can be computed by differentiating the ODE integrator). We used $K = 6000$ samples.

For MCMC, to be consistent with [Zhang & Chen \(2022\)](#), we generated 15000 samples, each of which was seen 30 times in training. We used 1000 steps of Metropolis-adjusted Langevin sampling with ϵ linearly decaying from 0.1 to 0.

The flow network used to generate Fig. 5 followed similar settings to those used in §6.1.

D.7. Unsupervised Translation

We trained a vanilla convolutional VAE, with about 7 million parameters in the encoder, on CelebA faces scaled to 128×128 resolution.

For the flow network $v_\theta(t, x)$, we used a MLP with four hidden layers of 512 units and leaky ReLU activations taking the 129-dimensional concatenation of x and t as input. All models CFM and OT-CFM were trained for 5000 batches of size 256 and the Adam optimizer with learning rate 10^{-3} . Integration was performed using the Dormand-Prince integrator with tolerance 10^{-3} . For each attribute, 1000 positive and negative images each were used as a held-out test set.

Figure S8 shows some examples of the learned trajectories.

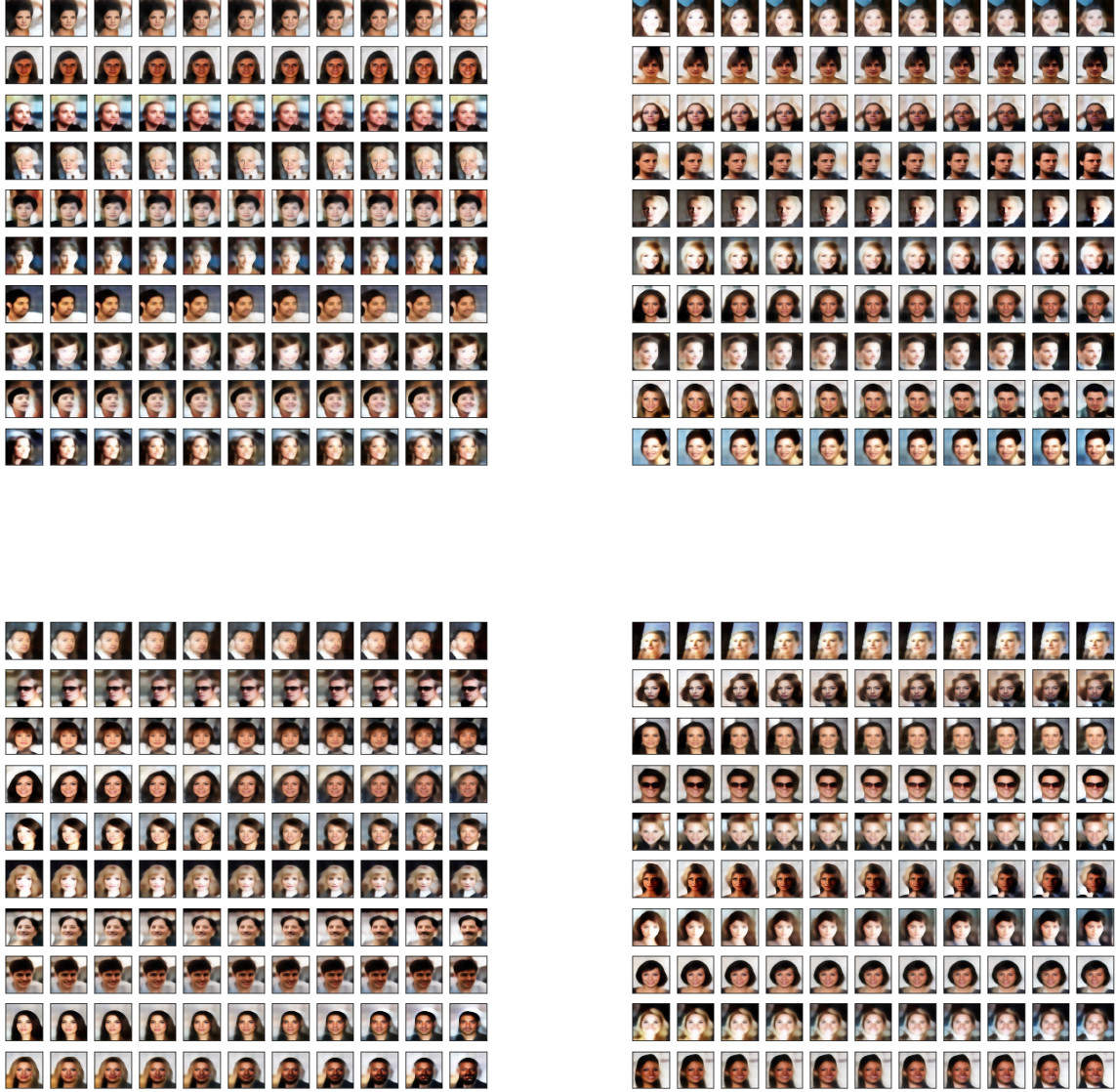


Figure S8. Image-to-image translation in the latent space of CelebA images: An OT-CNF is trained to translate between latent encodings of images that are negative and positive for a given attribute. The first column is a reconstructed encoding x_0 of a real negative image. The next ten columns are decodings of images along the flow trajectory with initial condition x_0 , with x_1 shown in the right column. **Top row:** not smiling \rightarrow smiling, not male \rightarrow male, showing the preservation of image structure and other attributes. **Bottom row:** no mustache \rightarrow mustache, not wearing necktie \rightarrow wearing necktie, showing partial failure modes. Both features are well-predicted by the latent vector, but infrequent in the dataset and highly correlated with other attributes, such as ‘male’, leading to unpredictable behaviour for out-of-distribution samples and modification of attributes different from the target.